Quaternary Research (2024), **117**, 135–159
doi:10.1017/qua.2023.53

Research Article

Limitations of precipitation reconstructions using equilibrium-line altitudes exemplified for former glaciers in the Southern Black Forest, Central Europe

Felix Martin Hofmann[a], Martin Steiner[a], Stefan Hergarten[a], ASTER Team[b,**] and Frank Preusser[a]

[a]Institute of Earth and Environmental Sciences, University of Freiburg, Albertstraße 23b, 79104 Freiburg, Germany and [b]Aix-Marseille Université, CNRS, IRD, INRAE, Technopôle de l'Environnement Arbois-Mediterranée, BP80, 13545 Aix-en-Provence, France

Abstract

To further elucidate the Late Pleistocene glacial history of mid-elevation mountainous regions in Central Europe, ^{10}Be cosmic-ray exposure (CRE) dating was applied to moraines in the Zastler Tal Valley in the Southern Black Forest. Periods of glacier recession from moraines in this valley began no later than 16 ka, 15 ka, and 13 ka. CRE ages of moraines in this and other parts of the Southern Black Forest cluster around 17–16 ka and 15–14 ka, thus suggesting a common forcing of glacier recession. Equilibrium-line altitudes (ELAs) during moraine formation were calculated for precipitation reconstruction. Observed spatial discrepancies in ELAs at ca. 15–14 ka are explained best by the size of snow-contributing areas. The reconstructed annual precipitation at the ELA for ca. 16 ka and ca. 15 ka is affected by large uncertainties, representing a wide range from ~50% to ~150% of present-day values. Due to various factors, such as drifting snow, the lower bounds of the estimates appear most realistic, thus concurring with the common hypothesis of less precipitation during the last glacial termination than today in Central Europe. Further research is needed before ELAs of small ice masses can be employed for precise precipitation estimates.

Keywords: Black Forest, Glacier, Moraine, Terrestrial cosmogenic nuclide dating, Equilibrium-line altitude

INTRODUCTION

During the final part of the Late Pleistocene (i.e., during Marine Oxygen Isotope Stage 2; 29–14 ka; Lisiecki and Raymo, 2005), large ice sheets developed in Europe over Scandinavia and the British Isles. A network of valley glaciers covered the Alps at the same time. Previous work showed that ice build-up and decay followed complex temporal and spatial patterns (e.g., Ivy-Ochs et al., 2008; Hughes and Gibbard, 2015; Gaar et al., 2019; Clark et al., 2022), apparently reflecting shifts of the position of the polar front over the North Atlantic (Florineth and Schlüchter, 2000; Kuhlemann et al., 2008; Monegato et al., 2017; Gribenski et al., 2021). Chronological data from moraines confirmed that, apart from these ice masses, ice caps and glaciers covered the currently ice-free, mid-elevation mountainous regions in Central Europe, including the Jura (Graf et al., 2015), the Vosges (Mercier et al., 1999), the Black Forest (Hofmann et al., 2022), the Bavarian Forest (Reuther, 2007), the Bohemian Forest (Mentlík et al., 2013), and the Giant Mountains (Mercier et al., 2000; Engel et al., 2011, 2014). The highest peaks in these regions reach maximum elevations between 1424 m (Vosges) and 1720 m (Jura) above sea-level (note that elevations are given in meters above present-day sea-level throughout this paper). Episodes of abrupt cooling punctuated the warming trend during the last glacial termination (see Heiri et al., 2014a, and Palacios et al., 2023, for overviews), which was the period between the last glacial maximum (at 27.5–23.3 ka; Hughes and Gibbard, 2015) and the onset of the Holocene (at 11.7 ka; Rasmussen et al., 2014). These cooling events (at ca. 14 ka and ca. 12.7 ka) led to glacial re-advances and standstills in mid-elevation mountainous regions in Central Europe (Mercier et al., 1999, 2000; Reuther, 2007; Engel et al., 2011, 2014; Mentlík et al., 2013; Hofmann et al., 2022).

Investigating past glaciations of mid-elevation mountainous regions in Central Europe (Fig. 1) may further refine our understanding of the mechanisms of Pleistocene climate change (cf., Heyman et al., 2013). While the evolution of summer temperatures during the last glacial termination has been quantified at multiple sites in and around the Alps through the investigation of chironomid assemblages (e.g., Heiri and Millet, 2005; Larocque-Tobler et al., 2010; Heiri et al., 2014b; Bolland et al., 2020), precipitation records are scarce (Guiot et al., 1989; Magny et al., 2001, 2006; Peyron et al., 2005). Rea et al. (2020) attempted to fill this gap by conducting a reconstruction of precipitation during the 12.9–11.7 ka period, often referred to as the Younger Dryas (Mangerud, 2021; Naughton et al., 2023). This reconstruction was based on temperature records from

Corresponding author: Felix Martin Hofmann; Email: felix.martin.hofmann@geologie.uni-freiburg.de

**Georges Aumaître, Karim Keddadouche, and Fawzi Zaidi

Cite this article: Hofmann FM, Steiner M, Hergarten S, ASTER Team, Preusser F (2024). Limitations of precipitation reconstructions using equilibrium-line altitudes exemplified for former glaciers in the Southern Black Forest, Central Europe. *Quaternary Research* **117**, 135–159. https://doi.org/10.1017/qua.2023.53

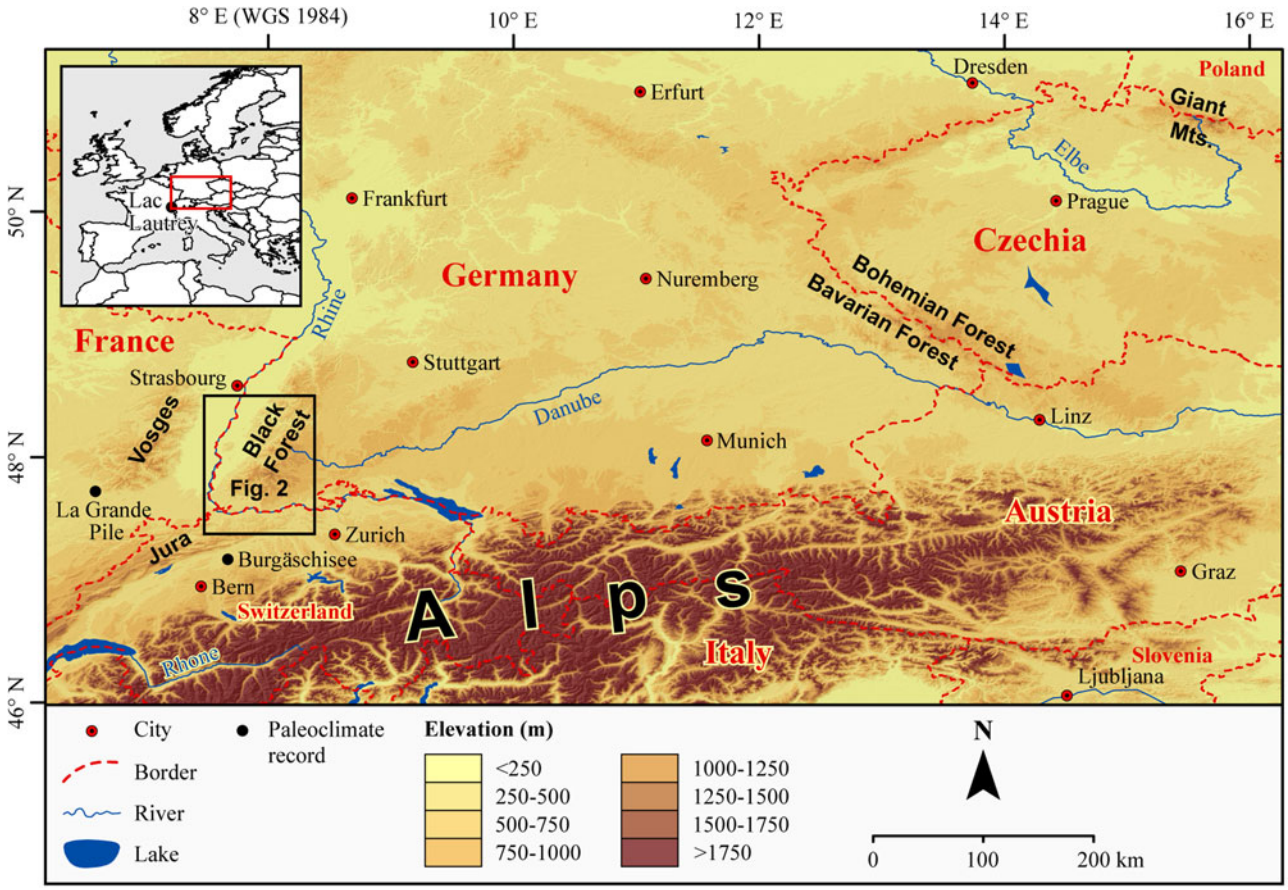

Figure 1. Topographic map of Central Europe showing sites discussed in the text. The digital elevation model in the background is a SRTM–DEM (shuttle radar topography mission–digital elevation model; Jarvis et al., 2008). ©EuroGeographics for administrative boundaries. ©European Environment Agency for rivers and lakes.

sites across Europe and on equilibrium-line altitudes (ELAs) of 122 glaciers (i.e., the zones of glaciers where net accumulation corresponded to net ablation over a period of one year; Bakke and Nesje, 2011). Because ablation and accumulation are linked to the summer temperature and annual precipitation, respectively (Ohmura and Boettcher, 2018), past precipitation at ELAs can be inferred with the aid of empirical relationships (Ohmura et al., 1992; Dahl et al., 1997; Ohmura and Boettcher, 2018), if summer temperature estimates are available from an independent record. However, for Central Europe, the study of Rea et al. (2020) is limited to only one cirque glacier in the Giant Mountains. Although Rea et al. (2020) did not provide uncertainties for their precipitation estimates, the annual precipitation at the ELA of this glacier during the 12.9–11.7 ka period (1435 mm/yr) was in the range of present-day values (~1500 mm/yr; Engel et al., 2014). Interestingly, it is still unclear whether other mid-elevation mountainous regions in Central Europe, such as the Vosges or the Southern Black Forest, were also glaciated during this cool period. Furthermore, reconstruction of precipitation during other periods of the last glacial termination would enhance our understanding of past circulation changes but it would require additional data on the temporal and spatial evolution of glaciers and ELAs. Small ice masses are particularly suitable for precipitation reconstruction due to their short response times to climatic oscillations and their high sensitivity to short-term climatic changes (Mackintosh et al., 2017). However, topoclimatic factors, such as shading, may significantly influence their mass balance and need to be considered (e.g., Coleman et al., 2009; Mills et al., 2009; Chandler and Lukas, 2017).

The Black Forest is situated in southwestern Germany (Fig. 1) and is commonly subdivided into a northern, central, and southern part. During the last Pleistocene glaciation, the Northern Black Forest (max. elevation: 1164 m) hosted a small icefield and numerous cirque glaciers (Fezer et al., 1961; Zienert and Fezer, 1967). Small cirque and valley glaciers covered areas at high elevation (max. elevation: ~1000 m) in the Central Black Forest (Reichelt, 1996). Because a significant portion of the Southern Black Forest is situated above 1000 m, this region was the most extensively glaciated. Previous studies concluded that this region temporarily hosted four, presumably interconnected ice caps and their outlet glaciers, covering altogether an area of about 1000 km^2 (Metz and Saurer, 2012). The largest ice cap rested on the highest summit, Feldberg (1493 m), and on the surrounding region (Fig. 2; cf., Hofmann et al., 2020). The outlet glaciers of this ice cap attained lengths of up to 25 km and a maximum thickness of 440 m (Sawatzki, 1992; Hemmerle et al., 2016). Three summits in the surrounding region (Belchen [1414 m], Köhlgarten [1224 m], and Schauinsland [1284 m]; Fig. 2) hosted significantly smaller ice caps (Giermann, 1964; Rahm, 1987).

Numerous moraines have been mapped inside the assumed Late Pleistocene maximum ice extent around Feldberg, Belchen,

https://doi.org/10.1017/qua.2023.53 Published online by Cambridge University Press

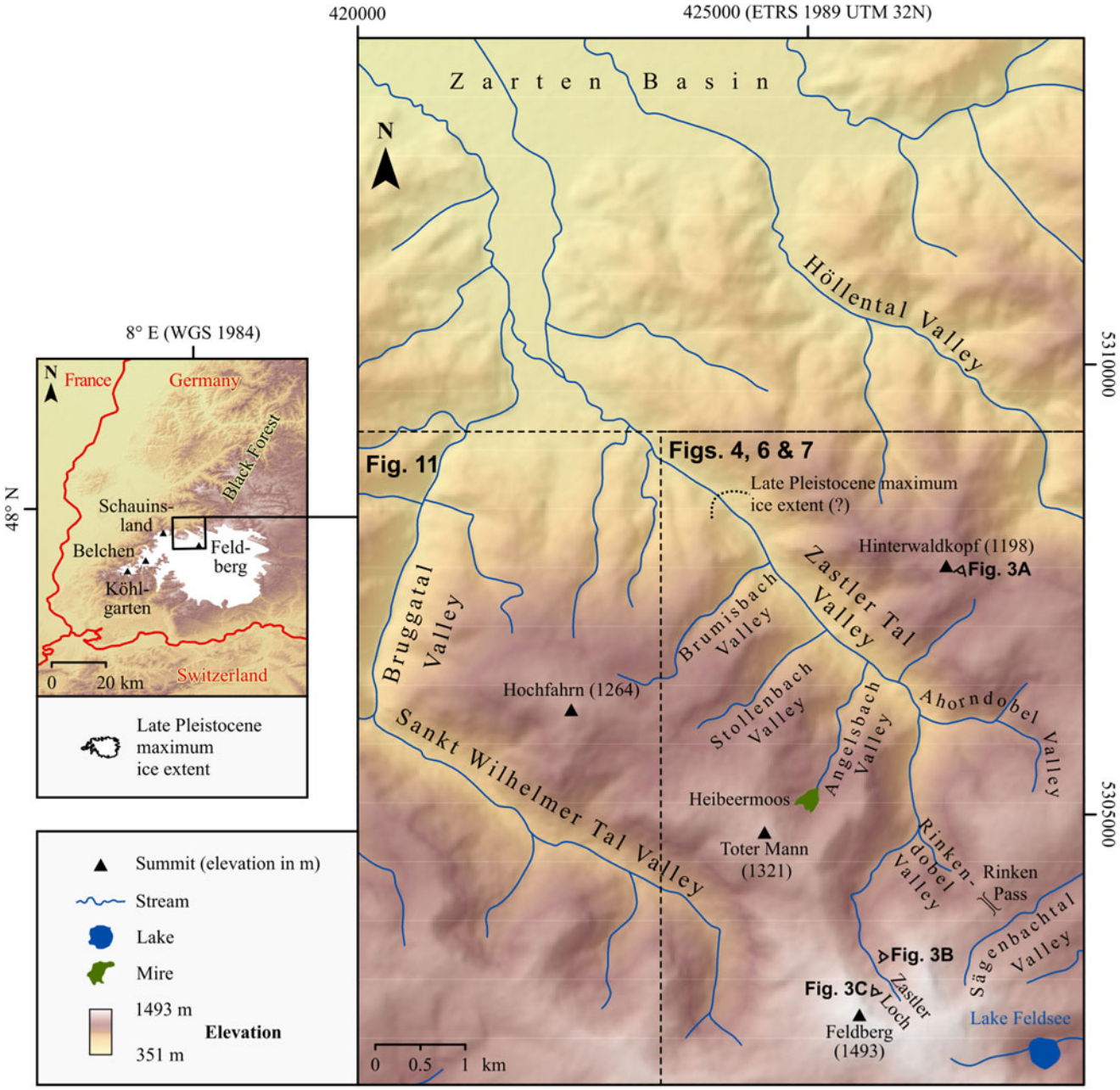

Figure 2. Location of the study area and map of the study area showing sites discussed in the text. The assumed Late Pleistocene maximum ice extent in the Southern Black Forest (Hemmerle et al., 2016) is shown in white. The DEM in the background was derived from data obtained during the SRTM (Earth Resources Observation and Science [EROS] Center, 2018). Photo locations/directions of view for Figure 3A–C shown as diagrammatic eyes.

Köhlgarten, and Schauinsland (Steinmann, 1902; Liehl, 1982; Metz and Saurer, 2012). These landforms indicate that the ice caps first decayed into valley glaciers with independent accumulation areas and then evolved into small cirque glaciers (Hofmann et al., 2020). ^{10}Be CRE ages for moraines of one valley glacier suggest successive standstills and/or re-advances during overall glacier recession (between ca. 17 ka and ca. 16 ka), while final glacier recession in two cirques began no later than 14 ka (Hofmann et al., 2022). Despite this recently published glacier chronology, Late Pleistocene glacier variations in the Southern Black Forest are not sufficiently understood for three reasons: (1) the onset of ice retreat from the last glaciation maximum position has not been dated (cf., Hofmann et al., 2022), but this would answer the question if it occurred simultaneously with Alpine glaciers and the European ice shields; (2) it is not clear whether the deglaciation chronology presented by Hofmann et al. (2022) is representative for the entire Southern Black Forest; and (3) glacier variations at the end of the last deglaciation are poorly constrained because the presumably youngest moraines in the Black Forest have not been dated. These landforms are situated in the Zastler Tal Valley north of Feldberg. Lang (2005) speculated that these moraines might have the same age as those of the Egesen stadial in the Alps, exposure dated to 13.5–11 ka at multiple sites across the Alps (cf., Ivy-Ochs et al., 2023).

For this study, previously mapped moraines in the Zastler Tal Valley and one of its tributary valleys were selected for ^{10}Be CRE

https://doi.org/10.1017/qua.2023.53 Published online by Cambridge University Press

dating to elucidate the spatial and temporal evolution of the glaciers during the last glaciation of the Black Forest in more detail. This study aims to determine the onset of glacier recession from the moraines of the Late Pleistocene glaciation maximum and to test the hypothesis of Lang (2005) that the presumably youngest moraines have an age of about 13–11 ka. Determining their age has important implications for the reconstruction of precipitation patterns during the last cool period of the Pleistocene (12.9–11.7 ka). ELAs during moraine formation were reconstructed for use in tandem with previously published July temperature estimates for precipitation reconstruction.

STUDY AREA AND PREVIOUS WORK

Regional setting

The Zastler Tal Valley consists of the Zastler Tal Valley sensu stricto, hereinafter referred to as the main valley, and its tributary valleys, the Brumisbach Valley, Stollenbach Valley, Angelsbach Valley, Ahorndobel Valley, and the Rinkendobel Valley (Fig. 2). The uppermost reach of the main valley, referred to as Zastler Loch, is situated on the northeastern flank of Feldberg. The main valley meets the Bruggatal Valley at an elevation of about 450 m and leads into the Zarten Basin east of the city of Freiburg. The Hochfahrn–Toter Mann Massif separates the study area from the Sankt Wilhelmer Tal Valley to the southwest, whereas the Hinterwaldkopf Massif delimits the study area to the northeast. The entire study area drains to the Rhine.

The study area is located in the crystalline part of the Black Forest, representing the basement of the Variscan orogeny (380–290 Ma). With the denudation of the orogen, various sediments were deposited on top of the crystalline basement under terrestrial and marine conditions during the Permian, Triassic, and Jurassic (cf., Geyer and Gwinner, 2011). Due to tectonic activity associated with the formation of the Upper Rhine Graben (starting at around 50 Ma; Ziegler, 1992), the Southern Black Forest was uplifted, and the Mesozoic sedimentary rocks were stripped off. Lithologies of the Variscan basement, such as migmatites, paragneisses, or orthogneisses, dominate the study area (Schreiner, 1996).

A subarctic climate prevails in the summit area of Feldberg (Dfc climate according to the Köppen climate classification). According to data of the German Weather Service (DWD), mean annual precipitation and mean annual temperature from 1961–1990 CE amounted to 1909 mm and 3.3°C at the weather station on Feldberg (at 1486 m), respectively (https://opendata.dwd.de; accessed 22 June 2023). Snowfall accounts for about two-thirds of the annual precipitation (Parlow and Rosner, 1997). Snow cover on Feldberg lasts, on average, for 157 days per year (Matzarakis, 2012). The climate at lower elevations than the summit area of Feldberg is classified as temperate (Cfb climate according to the Köppen climate classification). Elevation has a strong effect on the amount of annual precipitation, with mean annual precipitation increasing by 100 mm per 100 m in elevation (Parlow and Rosner, 1997).

Ice-marginal positions in the Zastler Tal Valley

Widespread glacial landforms and deposits in the Zastler Tal Valley document the strong imprint of Quaternary glaciations (Wimmenauer et al., 1990; Hann et al., 2011; Metz and Saurer, 2012). Glaciers covered the main valley and probably four of its tributary valleys (the Brumisbach Valley, Stollenbach Valley, Angelsbach Valley, and the Rinkendobel Valley; Liehl, 1982). Prominent examples of erosional glacial landforms are the stairway cirque in the main valley (Zastler Loch), the Angelsbach Cirque, and a whaleback in Zastler Loch (Fig. 3).

Ice-marginal moraines occur at elevations between 550 m and 1430 m in the main valley as well as in two of its tributary valleys, the Angelsbach Valley and the Rinkendobel Valley. They were first mapped by Steinmann (1902, 1910), whereas Erb (1948), Zienert (1973), Liehl (1975), and Schreiner (1977) identified additional moraines. Metz (1985a) later published a geomorphological map showing glacial landforms in the upper reaches of the study area. After the publication of two geological maps including the Zastler Tal Valley (Wimmenauer et al., 1990; Schreiner, 1996), interest in the glaciation of the study area markedly declined. Previous work on moraines in the Zastler Tal Valley was summarized by Liehl (1982), Metz and Saurer (2012), Hemmerle et al. (2016), and Hofmann et al. (2020).

The availability of high-resolution elevation data has led to a renewed interest in glacial landforms in the study area. Geomorphological mapping was recently undertaken with the aid of such data (Hofmann et al., 2020). Revisiting glacial landforms in the Zastler Tal Valley proved to be a prerequisite for this study because some of previously mapped moraines turned out to be landforms other than moraines, whereas some glacial landforms were mapped for the first time. Therefore, we refer to the study of Hofmann et al. (2020) in the following synthesis (see Fig. 4 for a map of moraines and ice-marginal positions).

The lowermost ice-marginal landform in the main valley is a short sediment ridge on the southwestern valley wall at an elevation of 540–600 m (ZT-18; Fig. 4). It has been tentatively mapped as an ice-marginal moraine (Erb, 1948; Hüttner, 1967; Hofmann et al., 2020). This landform has been considered indicative of the Late Pleistocene maximum ice extent in the Zastler Tal Valley (Fig. 2; Erb, 1948; Liehl, 1982; Metz and Saurer, 2012). A nearby sediment ridge has been interpreted as an ice-marginal moraine and ascribed to ice-marginal position ZT-17.

A prominent ice-marginal moraine is located at the northwestern end of a tongue basin farther upvalley (ice-marginal position ZT-16). According to Zienert (1973), this moraine represents the Late Pleistocene glaciation maximum in the Zastler Tal Valley. A ridge-shaped accumulation of boulders on the northeast-facing valley wall between the entrance to the Stollenbach Valley and Angelsbach Valley probably pertains to the same ice-marginal position (Hofmann et al., 2020, Fig. 13).

The moraines atice-marginal position ZT-15 are situated at around 640 m. A small ice-marginal moraine farther upvalley (at 720 m) documents ice-marginal position ZT-14. Two ice-marginal moraines are situated on the western valley wall near the entrance to the Rinkendobel Valley (ice-marginal positions ZT-13 and ZT-12). Two moraines on the eastern valley wall probably belong to the same ice-marginal positions (Fig. 4C). Two smooth moraines lie on the valley floor (ice-marginal positions ZT-11 and ZT-10). These moraines have been considered as old as two moraines on the eastern valley wall farther southeast (Fig. 4C).

The morphologically most prominent ice-marginal moraine in the entire main valley is a semi-circular, double-crested moraine complex at an elevation of 1030 m (at ice-marginal positions ZT-09 and ZT-08). The eastern part of the moraine complex is oriented parallel to the valley floor and progresses in a southerly direction farther upvalley.

An ice-marginal moraine is situated farther southeast on the eastern valley wall high above the valley floor (ice-marginal position ZT-07). An ice-marginal moraine on the eastern valley wall

https://doi.org/10.1017/qua.2023.53 Published online by Cambridge University Press

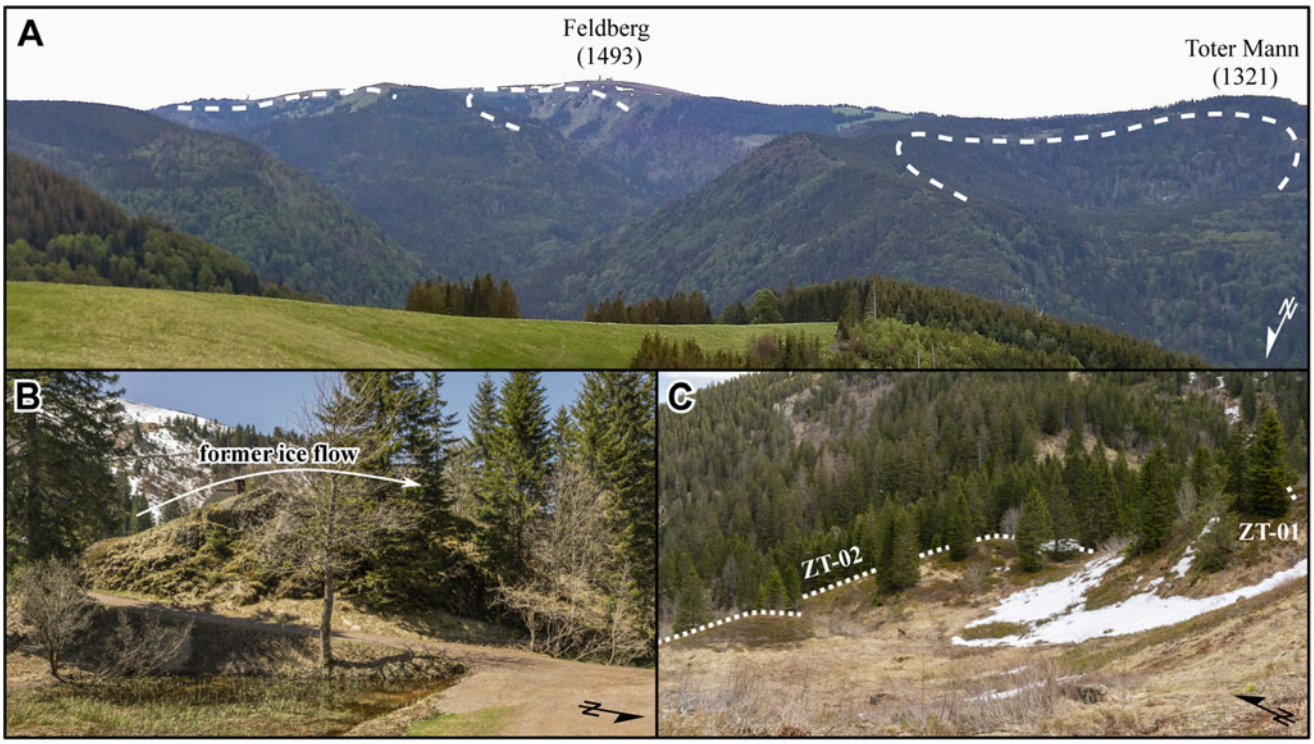

Figure 3. Examples of glacial landforms in the study area (elevations in m). (**A**) Panorama of the Zastler Tal Valley from Hinterwaldkopf. Three glacial cirques (marked with dashed lines) that are well recognizable from Hinterwaldkopf, from east to west, are the cirque in the upper reaches of the Sägenbachtal Valley, the stairway cirque in the uppermost part of the Zastler Tal Valley (Zastler Loch), and the Angelsbach Stairway Cirque. (**B**) Whaleback at an elevation of 1250 m in Zastler Loch. (**C**) Moraines at ice-marginal positions ZT-01 and ZT-02 (Hofmann et al., 2020) seen from the western headwall of Zastler Loch. See Figure 2 for the locations and view directions from where photos were taken (all photos: F.M. Hofmann).

and a moraine on the opposite valley wall have been ascribed to the next younger ice-marginal position ZT-06. Two rather small ice-marginal moraines lie on the eastern valley wall farther southeast. These landforms probably pertain to ice-marginal positions ZT-08 and ZT-05. The ice-marginal moraines at ice-marginal position ZT-04 are situated on the lowermost cirque floor of Zastler Loch. Lang (2005) correlated the moraines at ice-marginal positions ZT-04 and younger moraines with those ascribed to the Egesen stadial in the Alps (exposure dated to 13.5–11 ka; Ivy-Ochs et al., 2023).

An ice-marginal moraine is located at an elevation of 1340–1350 m on the western headwall of Zastler Loch. This landform is probably as old as an ice-marginal moraine farther east, hence these landforms are considered indicative of ice-marginal position ZT-03. The geometries of the crests of all moraines in younger morphostratigraphic positions (ice-marginal positions ZT-02 and ZT-01) suggest that the moraines formed at the margin of two different glaciers. A lobate series of ice-marginal moraines at 1320–1340 m documents ice-marginal position ZT-02 of a small glacier on the cirque's western headwall. The innermost ice-marginal position ZT-01 at this locality is documented by small ice-marginal moraines. Another set of moraines is situated on the uppermost cirque floor farther southeast (at 1400–1430 m). The moraines on the uppermost cirque floor (ice-marginal positions ZT-02 and ZT-01) are located at a significantly higher elevation than those on the western headwall.

Numerous moraines have been mapped in the Rinkendobel Valley and on the main ridge between the Rinkendobel Valley and the upper part of the Zastler Tal Valley. Because till covers the southward-facing slope north of Rinken Pass up to an elevation of 1240 m (Metz, 1985b; Wimmenauer et al., 1990; Schreiner, 1996), the moraines probably formed at the margin of an ice stream that advanced from the Sägenbachtal Valley over Rinken Pass into the Rinkendobel Valley. The lobate moraine in the southern glacial cirque west of Rinken Pass probably formed at the margin of a small cirque glacier (Liehl, 1975; Metz, 1985b).

The moraines in the Angelsbach Valley have been assigned to five ice-marginal positions (Fig. 4B). The moraine at ice-marginal position AB-05 is situated on the eastern valley wall. A double-crested moraine complex on the valley floor documents ice-marginal positions AB-04 and AB-03. This landform is probably as old as two ice-marginal moraines on the eastern valley wall farther south. The morphologically most prominent glacial landforms in the Angelsbach Cirque, the moraines at ice-marginal position AB-02, are situated farther upvalley. These moraines surround Heibeermoos, a peat bog in the former tongue basin in the Angelsbach Cirque (Fig. 4; Erb, 1948; Hann et al., 2011). An ice-marginal moraine is situated at the northern end of the southernmost cirque in the Angelsbach Valley. This landform documents ice-marginal position AB-01. Although initial cirques have been mapped in the upper reaches of the Stollenbach Valley and the Brumisbach Valley (Hofmann et al., 2020), these valleys are devoid of ice-marginal landforms.

METHODS

^{10}Be CRE dating

Fieldwork

During geomorphological field mapping for an earlier study (Hofmann et al., 2020), all suitable moraine boulders with a

https://doi.org/10.1017/qua.2023.53 Published online by Cambridge University Press

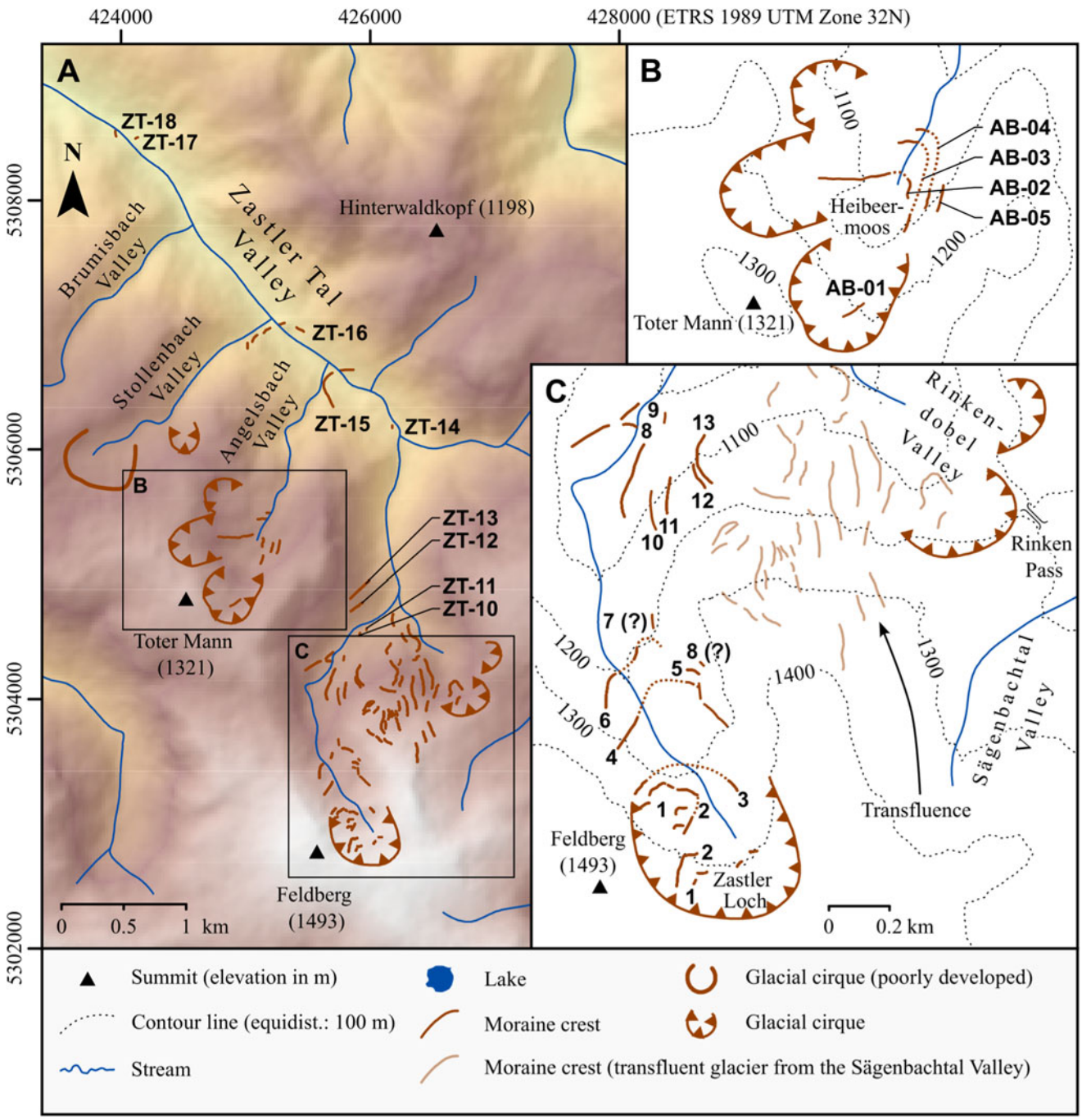

Figure 4. Glacial cirques, moraine crests and ice-marginal positions in the (**A**) Zastler Tal Valley, the (**B**) Angelsbach Cirque, and the (**C**) uppermost part of the Zastler Tal Valley and in the Rinkendobel Valley (Hofmann et al., 2020). See Figure 2 for the data source of the DEM in the background.

height of ≥ 1 m observed in the main valley as well as in the Angelsbach Cirque were sampled for ^{10}Be CRE dating. In an attempt to avoid complex exposure histories, we only selected boulders that were well embedded in moraines. Most of these boulders were not flat-topped, thus inclined rock surfaces with a constant angle were chosen. Rock surfaces near edges were avoided to prevent potential edge effects (Masarik and Wieler, 2003). The strike and dip of the selected sampling surfaces were recorded with a geological compass. The coordinates of sampling sites were determined with a handheld GPS. Rock samples (n = 18; Table 1) were obtained with the aid of a battery-powered saw and a chisel. A detailed sample documentation is given in the supplementary material.

Sample preparation and accelerator mass spectrometry measurements

Prior to sample preparation, the mass and thickness of each rock fragment in a sample was determined to compute the mass-weighted average of the sample's thickness. Quartz separation and ^{10}Be extraction from purified quartz were conducted in the laboratory facilities of the University of Freiburg (Germany) and the Laboratoire National des Nucléides Cosmogéniques

https://doi.org/10.1017/qua.2023.53 Published online by Cambridge University Press

Table 1. Characteristics of samples from moraine boulders in the Zastler Tal Valley. Sample numbers from the moraine boulders refer to the morphostratigraphic positions of the respective ice-marginal moraines.

Boulder	Latitude (°N WGS 1984)	Longitude (°E WGS 1984)	Elevation (m)	Boulder height (m)	Lithology	Sample thickness (cm)	Topographic shielding factor
AB-02a	7.995433	47.896071	1093	4.2	Gneiss	2.4	0.972
AB-02b	7.995483	47.896183	1097	2.3	Gneiss	2.7	0.967
AB-02c	7.996115	47.896704	1098	1.2	Gneiss	2.6	0.992
AB-02d	7.996802	47.896754	1084	1.0	Gneiss	2.5	0.961
AB-02e	7.998488	47.896565	1076	4.5	Gneiss	2.5	0.986
AB-03a	7.998589	47.897998	1072	1.5	Gneiss	1.9	0.994
AB-03b	7.998749	47.898034	1070	1.6	Migmatite	1.4	0.961
AB-03c	7.998212	47.898204	1068	2.1	Gneiss	1.8	0.992
ZT-04a	8.005514	47.878175	1310	1.6	Gneiss	2.1	0.882
ZT-04b	8.008877	47.879489	1260	2.1	Gneiss	2.3	0.965
ZT-04c	8.009660	47.879250	1283	1.7	Gneiss	3.1	0.960
ZT-04d	8.010148	47.879049	1292	1.7	Gneiss	3.1	0.956
ZT-04e	8.010194	47.879033	1292	1.8	Gneiss	2.5	0.850
ZT-08a-1	8.005556	47.887661	1034	1.4	Migmatite	2.4	0.979
ZT-08a-2	8.005556	47.887661	1034	1.4	Migmatite	2.3	0.979
ZT-08b	8.006341	47.886590	1046	1.1	Migmatite	3.0	0.973
ZT-15a-1	8.005326	47.908382	660	2.3	Gneiss	2.0	0.961
ZT-15a-2	8.005326	47.908382	660	2.3	Gneiss	2.0	0.960

(LN_2C) in Aix-en-Provence (France) according to a protocol adapted from Brown et al. (1991) and Merchel and Herpers (1999). After crushing, and wet sieving, the samples were passed through a magnetic separator (S.G. Frantz Co.). The samples were then treated with mixtures of 37% HCl and 35% H_2SiF_6 to further isolate quartz and remove feldspars. Because the samples still contained feldspar after this treatment, they were etched with diluted 5.5% HF, dried, spiked with magnetite powder (325 mesh) and passed through a magnetic separator. Atmospheric ^{10}Be was removed with 48% HF in three steps. In each step, 10% of the quartz was dissolved. About 150 mg of a ^{9}Be carrier solution (3025 ± 9 µg ^{9}Be/g) was added to each sample before total dissolution with 48% HF. Chromatography with anionic and cationic exchange resins (DOWEX 1X8 and 50WX8), as well as precipitation stages subsequently were conducted to further separate and purify beryllium. The final $Be(OH)_2$ precipitate was dried and oxidized at 700°C to obtain BeO.

Beryllium oxide was mixed with niobium powder and loaded into copper cathodes for accelerator mass spectrometry (AMS) measurements. AMS measurements were performed at the French national facility ASTER (Accélérateur pour les Sciences de la Terre, Environnement, Risques; Arnold et al., 2010) at CEREGE (Centre Européen de Recherche et d'Enseignement des Geosciences de l'Environnement) in Aix-en-Provence, France. Measured ^{10}Be/^{9}Be ratios were normalized with respect to the in-house standard STD-11 using an assigned ^{10}Be/^{9}Be ratio of $(1.191 \pm 0.013) \times 10^{-11}$ (Braucher et al., 2015) and the ^{10}Be half-life of $(1.387 \pm 0.012) \times 10^{6}$ years (Chmeleff et al., 2010; Korschinek et al., 2010). It should be noted that the STD-11 standard was calibrated by reference to the NIST_27900 standardization that is equivalent to the widely used KNSTD07 standardization (Nishiizumi et al., 2007) at rounding error (https://hess.ess.washington.edu/math/docs/al_be_v22/AlBe_standardization_table.pdf; accessed 30 June 2023). The ^{10}Be/^{9}Be ratio uncertainty in Table 2 includes the measurement uncertainty (counting statistics), the uncertainty of average standard measures, and the systematic error of ASTER (0.5%; Arnold et al., 2010). ^{10}Be concentrations in rock samples (Table 2) were corrected with the ^{10}Be concentration in a batch-specific chemical blank (measured ^{10}Be/^{9}Be ratio: $[0.125 \pm 0.021] \times 10^{14}$; number of added ^{9}Be atoms: $[2.98355 \pm 0.02208] \times 10^{19}$; ^{10}Be concentration: 37264 ± 6365 atoms ^{10}Be).

CRE age calculations

The elevations of the sampling sites were retrieved from a digital elevation model of the study area with x-y resolution of 1 m derived from light detection and ranging (LiDAR) data of the Baden–Württemberg State Agency for Spatial Information and Rural Development. Topographic shielding is commonly determined by approximating the horizon with a series of points and straight lines between them. Pairs of azimuth and elevation angles are recorded with an inclinometer as well as a compass and subsequently converted into a shielding factor (Li, 2013, 2018; Hofmann, 2022). This approach could not be applied to most sampling sites in the study area because most boulders were situated in dense forests where the horizon was not visible. Therefore, topographic shielding factors were computed with an ArcGIS toolbox (Li, 2018). As recommended by Hofmann (2022), the high-resolution digital elevation model was resampled to x-y resolution of 30 m for shielding factor calculations.

Apparent CRE ages in ka (kiloyears before 2010 CE) as well as internal (analytical) and external uncertainties (analytical

https://doi.org/10.1017/qua.2023.53 Published online by Cambridge University Press

Table 2. Results of Be measurements and cosmic-ray exposure ages of moraine boulders in the Angelsbach Cirque (AB) and in the Zastler Tal Valley sensu stricto (ZT). ^{10}Be concentrations in samples were corrected with the ^{10}Be concentration in a batch-specific chemical blank (37,264 ± 6365 atoms ^{10}Be). *During AMS measurements, ^{9}Be currents strongly decreased from 3.8 μA to 0.2 μA, therefore the age should not be considered reliable. **During Be measurements, Be currents dropped from 1.6 μA to 0.3 μA, therefore the age stated here should not be considered robust.

Sample	Mass of dissolved quartz (g)	^{9}Be-spike added (× 10^{19} atoms)	^{10}Be/^{9}Be ratio (× 10^{-14})	^{10}Be concentration & uncertainty (atoms/g quartz)	^{10}Be CRE age and internal uncertainty in ka (external uncertainties in parentheses)	
					uncorrected	corrected for postglacial denudation and snow shielding
AB-02a	8.7922	2.97950	3.326 ± 0.181	108467 ± 5220	11.01 ± 0.51 (0.57)	11.54 ± 0.53 (0.60)
AB-02b	12.4745	3.07855	5.839 ± 0.188	141116 ± 4143	14.30 ± 0.41 (0.53)	15.09 ± 0.42 (0.55)
AB-02c	6.8480	3.06238	2.561 ± 0.137	109064 ± 4946	10.82 ± 0.47 (0.53)	11.34 ± 0.49 (0.56)
AB-02d	16.7900	3.07451	7.365 ± 0.447	132654 ± 7726	13.66 ± 0.77 (0.84)	14.40 ± 0.81 (0.87)
AB-02e	9.2448	2.97748	5.059 ± 0.255	158899 ± 7422	15.97 ± 0.71 (0.81)	16.93 ± 0.77 (0.86)
AB-03a	12.6111	2.77332	7.014 ± 0.876	151288 ± 18420	15.09 ± 1.77 (1.81)*	15.95 ± 1.88 (1.91)*
AB-03b	16.7463	2.76726	8.501 ± 0.273	138250 ± 4193	14.25 ± 0.42 (0.53)	15.05 ± 0.43 (0.56)
AB-03c	9.4385	3.07249	5.303 ± 0.287	168681 ± 8525	16.84 ± 0.82 (0.91)	17.88 ± 0.88 (0.96)
ZT-04a	10.5124	2.99163	6.178 ± 0.437	172263 ± 11639	16.00 ± 1.04 (1.10)**	16.96 ± 1.10 (1.17)**
ZT-04b	11.5569	2.96131	5.657 ± 0.250	141730 ± 5790	12.60 ± 0.50 (0.59)	13.29 ± 0.53 (0.61)
ZT-04c	14.2126	3.06440	3.741 ± 0.153	78049 ± 2801	7.04 ± 0.24 (0.29)	7.32 ± 0.25 (0.30)
ZT-04d	8.7185	2.96738	4.216 ± 0.159	139234 ± 4623	12.28 ± 0.40 (0.49)	12.93 ± 0.42 (0.52)
ZT-04e	7.7970	3.18164	3.678 ± 0.151	145322 ± 5223	14.31 ± 0.49 (0.60)	15.11 ± 0.52 (0.62)
ZT-08a-1	11.0001	3.05632	4.703 ± 0.211	127293 ± 5215	13.40 ± 0.53 (0.62)	14.12 ± 0.56 (0.65)
ZT-08a-2	21.2308	3.05632	8.268 ± 0.389	117267 ± 5276	12.34 ± 0.54 (0.61)	12.98 ± 0.58 (0.65)
ZT-08b	10.8174	3.00982	3.870 ± 0.141	104232 ± 3283	11.03 ± 0.34 (0.42)	11.56 ± 0.35 (0.44)
ZT-15a-1	11.5496	2.99770	4.618 ± 0.179	116639 ± 4048	16.93 ± 0.57 (0.69)	17.99 ± 0.60 (0.74)
ZT-15a-2	12.3512	2.94716	4.667 ± 0.170	108340 ± 3516	15.77 ± 0.50 (0.61)	16.71 ± 0.53 (0.65)

uncertainties plus the error of the ^{10}Be production rate added in quadrature) were calculated with the online cosmic-ray exposure program (CREp; Martin et al., 2017), which is available at https://crep.otelo.univ-lorraine.fr (accessed 16 May 2022). The ^{10}Be production rate deduced from rock samples of the Chironico landslide in southern Switzerland (Claude et al., 2014) was selected because the landslide was the closest production-rate reference site to the study area. Time-dependent 'Lm' scaling (Nishiizumi et al., 1989; Lal, 1991; Stone, 2000; Balco et al., 2008) and the ERA atmosphere model (Uppala et al., 2005), as recommended by Martin et al. (2017), were selected in CREp to scale the ^{10}Be production rate to sampling sites. The ages were corrected for changes in Earth's magnetic field with data from an atmospheric ^{10}Be-based geomagnetic database (Muscheler et al., 2005). Selecting these parameters led to a production rate of 4.10 ± 0.10 atoms ^{10}Be/g quartz/yr at sea-level and high latitudes (SLHL), thus concurring with the global production rate in CREp (4.11 ± 0.19 atoms ^{10}Be/g quartz/yr at SLHL). Since the sampled boulders were quartz rich, the density of quartz (2.65 g/cm^3) was assumed to perform the thickness correction.

Because no protruding quartz veins were observed on the sampled boulders, we were unable to calculate sampling site-specific denudation rates for CRE age calculations. Reuther (2007) proposed a denudation rate of 0.24 cm/ka for a similar lithological and environmental setting in the Bavarian Forest (Fig. 1; recalculated with CREp and the parameters listed previously). Incorporating this (recalculated) denudation rate yielded, on average, 2.7% older ages. The age difference was largest for the ZT-15a-1 boulder (3.4%).

The ^{10}Be production rate from the Chironico landslide is affected by snow-cover bias but is not accounted in CREp. Because almost all sampling sites in the study area lie at a much higher elevation than the Chironico landslide (~800 m), snow cover is likely more important for our study. According to field observations, the sampled boulders were covered in winter by a few decimeters of snow, which is not easily removed by wind in forested areas. According to data from the weather station of the German Weather Service in the municipality of Titisee (at 846 m), situated east of the study area, seasonal snow cover lasted, on average, for four months in the 1961–1990 CE period (average snow thickness : 30 cm). Assuming similar snow cover on the sampled boulders during the whole duration of exposure, a snow density of 0.3 g/cm^3, an attenuation length for fast neutrons in snow of 109 g/cm^2 (Zweck et al., 2013), and the commonly used equation 3.76 of Gosse and Phillips (2001), an additional snow shielding factor of ~0.974 is suggested. Incorporating this factor during age calculations yields ages older by 2.6% on average.

Correcting the ages for both denudation and snow shielding leads to ages that are older by 5.4% on average (Table 2). These considerations imply that the ages presented here may be underestimated by a few centuries. However, because we cannot prove

https://doi.org/10.1017/qua.2023.53 Published online by Cambridge University Press

that the corrections for snow shielding and postglacial denudation are correct, we present both uncorrected (minimum estimate) and corrected exposure ages (Table 2).

Statistical assessment of ages

Where possible, multiple boulders were sampled at individual ice-marginal positions to detect potential under- and overestimated ages. The assessment of ages follows the procedure in Hofmann et al. (2022): if three or more ages were available from the same landform, reduced chi-squared (χ^2_R) was computed. χ^2_R was compared with a critical value from a standard χ^2-table (degrees of freedom = n–1). The confidence interval was set to 95%. If χ^2_R was lower than the critical value, the hypothesis that the data form a single population is at 95% confidence (Balco, 2011). In this case, the landform age corresponds to the arithmetic mean of the ages. The mean internal uncertainty of the ages plus the production rate error added in quadrature was defined as landform age uncertainty. If χ^2_R exceeded the critical value, measurement uncertainties did not fully account for scatter in ages from the same landform (Balco, 2011). In this case, the age that was farthest from the average age in relation to its measurement uncertainty was considered an outlier. This procedure was repeated until the remaining ages yielded an acceptable χ^2_R value. No more than half of the ages from the same landform were excluded. The landform age was determined by calculating the arithmetic mean of the remaining ages. The landform age uncertainty corresponds to the mean internal uncertainty of the remaining ages and the production rate error (2.4%) added in quadrature.

Glacier reconstructions and ELA calculations

Reconstructing ELAs of a former glacier provides valuable insights into the paleoclimate if the glacier's mass balance was predominantly controlled by temperature and precipitation (Mackintosh et al., 2017). Common methods for reconstructing ELAs are the accumulation area ratio (AAR) and the area–altitude balance ratio (AABR) methods (Pearce et al., 2017). In contrast to the former, the latter explicitly takes the hypsometry of a glacier into account (Osmaston, 2005) and was therefore adopted for this study.

This approach required glacier-surface reconstructions. For establishing DEMs of former glacier surfaces, the GlaRe toolbox for the ESRI ArcGIS software was chosen (Pellitero et al., 2016). For the first step, flowlines of former glaciers were created in ArcMap 10.8.1 and points with a spacing of 50 m were created along the flowlines. To calculate ice thickness, the basal shear stress needed to be provided at these points. Pellitero et al. (2016) suggested adjusting the basal shear stress progressively until the reconstructed ice thickness agrees with the position of ice-marginal landforms, such as moraines. In most cases, ice-marginal landforms have only been preserved close to former positions of glacier fronts. In these areas, the basal shear stress could be adjusted to tune glacier surfaces to geomorphological evidence. In all remaining areas, the default value of the GlaRe toolbox was used (100,000 Pa).

In topographically constrained areas, resistance to glacier flow can be provided by lateral drag (Benn and Hulton, 2010). Dimensionless shape factors (f) for points in topographically constrained areas were deduced from automatically created cross sections and ice thicknesses were recalculated. Contour lines of modern surfaces were derived from a resampled version of the high-resolution digital terrain model of the study area (x-y resolution = 5 m). Contour lines of former glaciers were drawn by hand. Following the approach of Sissons (1974), concave and convex contour lines were drawn in the suspected accumulation and ablation areas, respectively. DEMs of former glacier surfaces were established by applying the 'from contour to DEM' tool in the ELA calculation toolbox of Pellitero et al. (2015).

In an earlier study on the Late Pleistocene glaciation of the Southern Black Forest (Hofmann et al., 2022), ELAs were calculated with balance ratios for the Alps. Since we aimed to reconstruct annual precipitation at the ELA based on a precipitation/temperature function derived from data from modern glaciers across the world, ELAs were calculated with the global AABR to ensure consistency. Oien et al. (2022) demonstrated that the mean global AABR (1.75; presented by Rea, 2009) is statistically invalid and proposed that the median global AABR of 1.56 should be used for ELA calculations. Therefore, ELAs in the study area were calculated with a balance ratio of 1.56. The recently published AABR–ELAs of former glaciers in the Southern Black Forest (Hofmann et al., 2022) that were calculated with a balance ratio of 1.59 were recalculated with the median global AABR, leading to subtle shifts in ELAs.

Oien et al. (2022) found that the absolute median difference between ELAs calculated with the median global balance ratio and the actual ELAs of glaciers across the world amounts to 65.5 m. They argued that this difference can be regarded as potential error associated with calculated AABR–ELAs. The error of the ELA calculation is half of the interval chosen for ELA calculations (Pellitero et al., 2015). Because the interval was set to 2 m for this study, the error of the ELAs amounts to 1 m. This value and the potential error associated with the calculated AABR–ELAs were added in quadrature to determine the total ELA uncertainty. It should be noted that total ELA uncertainties only comprise the error associated with the AABR method.

ELA-based precipitation reconstruction

According to a global dataset compiled by Ohmura and Boettcher (2018), winter accumulation plus summer precipitation (P_a) in mm/yr at the ELA is related to the 3-month summer temperature (T_3) in the free atmosphere (°C) (i.e., the June, July, and August temperature in the northern hemisphere) which is:

$$P_a = 5.87 \times T_3^2 + 230 \times T_3 + 966$$

The standard error of this relationship amounts to 648 mm/yr (Ohmura and Boettcher, 2018).

The suitability of temperature/precipitation (P/T) relationships at ELAs of modern glaciers for formerly glaciated areas has been vigorously debated (e.g., Golledge et al., 2008, 2010; Boston et al., 2015; Chandler et al., 2019). Golledge et al. (2008, 2010) argued that the P/T function of Ohmura et al. (1992) ignores the principle of continentality. Indeed, the equations of both Ohmura et al. (1992) and Ohmura and Boettcher (2018) were derived from a global dataset of glaciers in various climatic regimes, including strongly maritime and continental Arctic settings. Increased seasonality results in a shorter ablation season (Hughes and Braithwaite, 2008), hence both equations will lead to an overestimation of accumulation or precipitation in settings with a highly continental climate. Climatic reconstructions point to extreme seasonality in Europe during the last glacial termination (Isarin and Renssen, 1999; Renssen and Isarin, 2001; Denton et al.,

https://doi.org/10.1017/qua.2023.53 Published online by Cambridge University Press

2005, 2010; Schenk et al., 2018). To the best of our knowledge, no relationship between summer temperatures and precipitation at the ELA has been proposed for the last glacial termination in Central Europe. Owing to the lack of a suitable alternative, the equation of Ohmura and Boettcher (2018) was adopted for this study.

Unfortunately, no July temperature record is available for the last glacial termination in the Black Forest. The closest site to the study area for which July temperatures have been inferred from chironomid assemblages is Burgäschisee on the Swiss Plateau (situated ~80 km south-southwest of the study area; Fig. 1). The recently published Burgäschisee July temperature record (Bolland et al., 2020) encompasses the period from ca. 18.4 ka to ca. 14.1 ka. The July temperature reconstruction for Lac Lautret (Jura; Fig. 1) for the 16.0–11.1 ka period (Heiri and Millet, 2005) was not used for two reasons. First, the reconstructed July temperatures for both sites (adjusted to an elevation of 1000 m assuming a lapse rate of 0.007 K/m; Kuttler, 2013) differ significantly in the 16.0–14.1 ka period, with an offset of up to ~5°C. As discussed by Heiri et al. (2015), this offset might be due to microclimatological/topographical effects that are known to affect water temperatures of lakes or regional differences in temperatures. Second, Lac Lautret is located about 220 km to the southwest of the study area and therefore likely less representative for the Southern Black Forest than Burgäschisee. Since the CRE ages of ice-marginal positions ZT-08 and ZT-04 did not overlap with the Burgäschisee record, we were able to reconstruct only annual precipitation at the ELA for ice-marginal positions ZT-15, AB-03, and AB-02. Due to the high temporal resolution of the record, multiple July temperature values matched the (minimum) landform ages. The lowest July temperature in the record that overlaps with the CRE ages of ice-marginal positions was extracted to reconstruct annual precipitation during moraine formation. This approach is based on the idea that periods of glacier expansion and moraine emplacement often coincide with climatically cool phases.

The P/T function of Ohmura and Boettcher (2018) requires T_3 instead of the mean July temperature. Rea et al. (2020, fig. S7) proposed a sound approach to convert the mean July temperature into T_3. They assumed that average monthly temperatures are best described by a sinusoidal function and obtained T_3 by fitting such a function through any two of the average annual temperature, the mean temperature of the coldest month, or the average temperature of the warmest month.

For this study, sinusoidal functions were established for the sampled ice-marginal positions based on the July temperature at the ELA and the annual temperature range. For each ice-marginal position, the average July temperature at Burgäschisee was adjusted to the ELA of each ice-marginal position assuming a 6.5°C/km lapse rate (ISO 2533:1975; https://www.iso.org/standard/7472.html). During the last glacial termination, the annual temperature range (i.e., the difference between the average temperatures of the coldest and warmest month) in Central Europe amounted to about 30°C (Isarin et al., 1998; Isarin and Renssen, 1999; Renssen and Isarin, 2001; Denton et al., 2005, 2010).

The following sinusoidal function allows for determining T_3 with the aid of data on July temperature at Burgäschisee and the assumed annual temperature range:

$$T = T_{mean} - A \times \cos\left(2\pi \times \frac{t - 0.5}{12}\right)$$

with

$$T_{mean} = \frac{T_{January} + T_{July}}{2} = T_{July} - \frac{\delta T}{2}$$

and

$$\delta T = T_{July} - T_{January}$$

where T is the temperature (°C), T_{mean} is the mean annual temperature (°C), A is the amplitude, t is the time (months), $T_{January}$ is the mean January temperature (°C), T_{July} is the mean July temperature (°C), and δT is the annual temperature range (°C).

It should be noted that $A \neq \frac{\delta T}{2}$, because δT refers to the mean July and January temperature. Instead,

$$A = \frac{\delta T}{\frac{\frac{\pi}{12} \times \sin\left(\frac{\pi}{12}\right)}{2}}$$

which is recognized by integrating the sinusoidal function from $t = 6$ months to $t = 7$ months.

Mean summer temperature was then obtained as follows:

$$T_3 = T_{mean} + \frac{\delta T}{\frac{\frac{\pi}{12} \times \sin\left(\frac{\pi}{12}\right)}{2}} \times \frac{12}{3\pi} \times \sin\left(\frac{3\pi}{12}\right)$$

The approach for the determination of T_3 is demonstrated for ice-marginal position AB-02 in Figure 5.

The error of T_{July} at the ELA was determined by multiplying the uncertainty of the ELA with the 6.5°C/km lapse rate (ISO

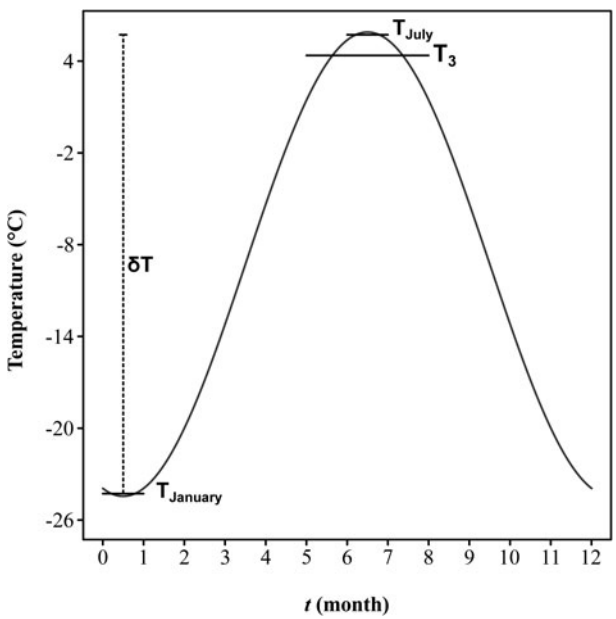

Figure 5. Determination of the mean summer temperature demonstrated for ice-marginal position AB-02. Average summer temperature was obtained by fitting a sinusoidal function with the aid of the mean July temperature and the annual temperature range. $t = 0$ corresponds to the first of January.

https://doi.org/10.1017/qua.2023.53 Published online by Cambridge University Press

2533:1975; https://www.iso.org/standard/7472.html). This value and the error of T_{July} were subsequently added in quadrature.

Annual precipitation subsequently was calculated with the P/T function of Ohmura and Boettcher (2018). To account for (1) the uncertainty of the P/T function of Ohmura and Boettcher (2018) and (2) the error of T_3 (δT_3), the uncertainty of P_a (δP) was determined by adding the standard error of the P/T function (648 mm/yr) and the derivation of the P/T function (multiplied by the uncertainty of T_3) in quadrature:

$$\delta P = \sqrt{[(11.74 \times T_3 + 230) \times \delta T_3]^2 + 648^2}$$

To be able to compare reconstructed P_a with present-day P_a, annual precipitation in the 1961–1990 CE period around the ELAs of former glaciers was retrieved from gridded precipitation data of the DWD (spatial resolution = 1000 m; available at https://opendata.dwd.de; accessed 22 June 2023).

Reconstruction of potential snow-blow and avalanche areas

In general, topoclimatic factors on snow accumulation (snow blow and avalanching) and ablation (topographic shading from incoming solar radiation) exert a particularly strong control on spatially restricted glaciations (Plummer and Phillips, 2003; Coleman et al., 2009; Mills et al., 2012). These factors may significantly influence mass balances and, thus, ELAs (e.g., Mitchell, 1996; Mills et al., 2009; Chandler and Lukas, 2017). The Angelsbach Cirque has a northeasterly aspect. Areas with a relatively subdued relief exist to the southwest of the cirque. Wind from the southwest and avalanching from the headwall of the cirque conceivably could have transported substantial amounts of snow to the cirque glacier during formation of the moraines in the cirque. Both proxy-based reconstructions and model simulations indicate that, during the last glacial termination, winds from the southwest were dominant over the southern part of Central Europe during winter (Renssen et al., 2007). Under the assumption of predominant surface winds from the southwest during winter, the conditions were favorable for snow blow from the southwest. This would have two main implications for the reconstruction of annual precipitation: (1) ELAs of glaciers in the cirque would lie below the climatic ELA (Bakke and Nesje, 2011), and (2) ELA-inferred annual precipitation for ice-marginal positions AB-03 and AB-02 would be overestimated.

To evaluate whether these factors exerted control on the former glacier in the Angelsbach Cirque, the potential snow-blow and avalanche areas during emplacement of the moraines at ice-marginal position AB-02 were reconstructed with established approaches (Mitchell, 1996; Mills et al., 2009; Chandler and Lukas, 2017). We restricted this reconstruction to ice-marginal position AB-02 and ice-marginal positions in the neighboring Sankt Wilhelmer Tal Valley for two reasons. First, the CRE age of ice-marginal position AB-02 matches well those of ice-marginal positions SW-02, SW-03, KS-01, KS-02, and KS-03 (ca. 14 ka) in the Sankt Wilhelmer Tal Valley to the southwest of the study area. Second, the moraines at ice-marginal position AB-02 in the Angelsbach Cirque lie in a similar morphostratigraphical position to those at ice-marginal positions WB-01, WB-02, and WB-03 in the Sankt Wilhelmer Tal Valley. Hofmann et al. (2022) already noted that, at ca. 14 ka, there was probably an ELA gradient across the Sankt Wilhelmer Tal Valley. They calculated lower ELAs during moraine formation for ice-marginal positions KS-01, KS-02, and KS-03 (~1150 m) than for ice-marginal positions WB-01, WB-02, WB-03, SW-02, and SW-03 (~1200 m). The cirque glaciers in the Sankt Wilhelmer Tal Valley at ca. 14 ka and the Angelsbach Cirque lay in a roughly 4 × 3 km area and, therefore, differences in temperature and precipitation across this area were probably very minor. The x-y coordinates of the midpoints of ELAs (coordinate system: ETRS 1989 UTM 32N) were plotted against ELAs to evaluate whether there was a W–E or N–S gradient in ELAs. We did not observe any clear spatial trend in ELAs across this area.

The lack of a clear spatial pattern called for assessment of the influence of topoclimatic effects on ELAs. Reconstructing potential snow-blow and avalanche areas of seven cirque glaciers in a relatively compact area (roughly 4 × 3 km) allowed us to assess whether differing ELAs of cirque glaciers could be explained by the varying sizes of potential snow-blow and avalanche areas. This analysis was based on the implicit assumption that the ELAs for ice-marginal positions were synchronous. We are aware that this might not have been the case.

The reconstruction of potential snow-blow areas was based on the assumption that the mass balances of glaciers were influenced by snow blow from all ground above the ELA, which was laterally continuous to glaciers. Following Chandler and Lukas (2017), the reconstructed potential snow-blow areas also comprised relatively flat areas above the ELA with a slope angle of ≤ 10°, irrespective of orientation. This threshold was used because areas with a slope angle of more than 10° dipping away from glacier surfaces may act as snow-fences (Chandler and Lukas, 2017, citing Robertson, 1988). Since surface winds from the southwest were dominant during winter at around 15 ka (Renssen et al., 2007), only potential snow-blow areas in a southwestern quadrant (180–270°) of glacier surfaces were included during the reconstruction of potential snow-blow areas, as has been done elsewhere (e.g., Benn and Ballantyne, 2005; Ballantyne, 2007). Potential avalanche areas encompassed all areas with a slope angle of ≥ 20° uphill from glacier surfaces (Chandler and Lukas, 2017).

Following the approach of Mitchell (1996), the significance of reconstructed potential snow-blow areas and potential avalanche areas was assessed by calculating the ratios of potential snow-blow area to glacier area (snow-blow ratios) and potential avalanche area to glacier area (avalanche ratio). Since not all ground inside potential snow-blow areas equally contributes snow to glaciers, Sissons (1980) proposed calculating snow-blow factors by taking the square root of the ratios of potential snow-blow area to glacier area. This approach was adopted for this study. Following the approach of Ballantyne (2007), who observed that potential snow-blow areas and potential avalanche areas frequently overlap, snow-blow and avalanching areas were merged into snow-contributing areas. Ratios of potential snow-contributing areas to glacier surfaces (avalanche and snow-blow ratios) were finally calculated.

RESULTS

CRE ages

We cannot unequivocally prove that the corrections for snow shielding and postglacial denudation are appropriate, therefore we present minimum exposure ages of individual boulders and landform ages (Figs. 6, 7). In addition, we report corrected ages in Table 2. See Table 3 for landform ages and χ^2_R values.

No sufficiently large and stable boulders were observed on the moraines at ice-marginal positions ZT-18 and ZT-17. The

https://doi.org/10.1017/qua.2023.53 Published online by Cambridge University Press

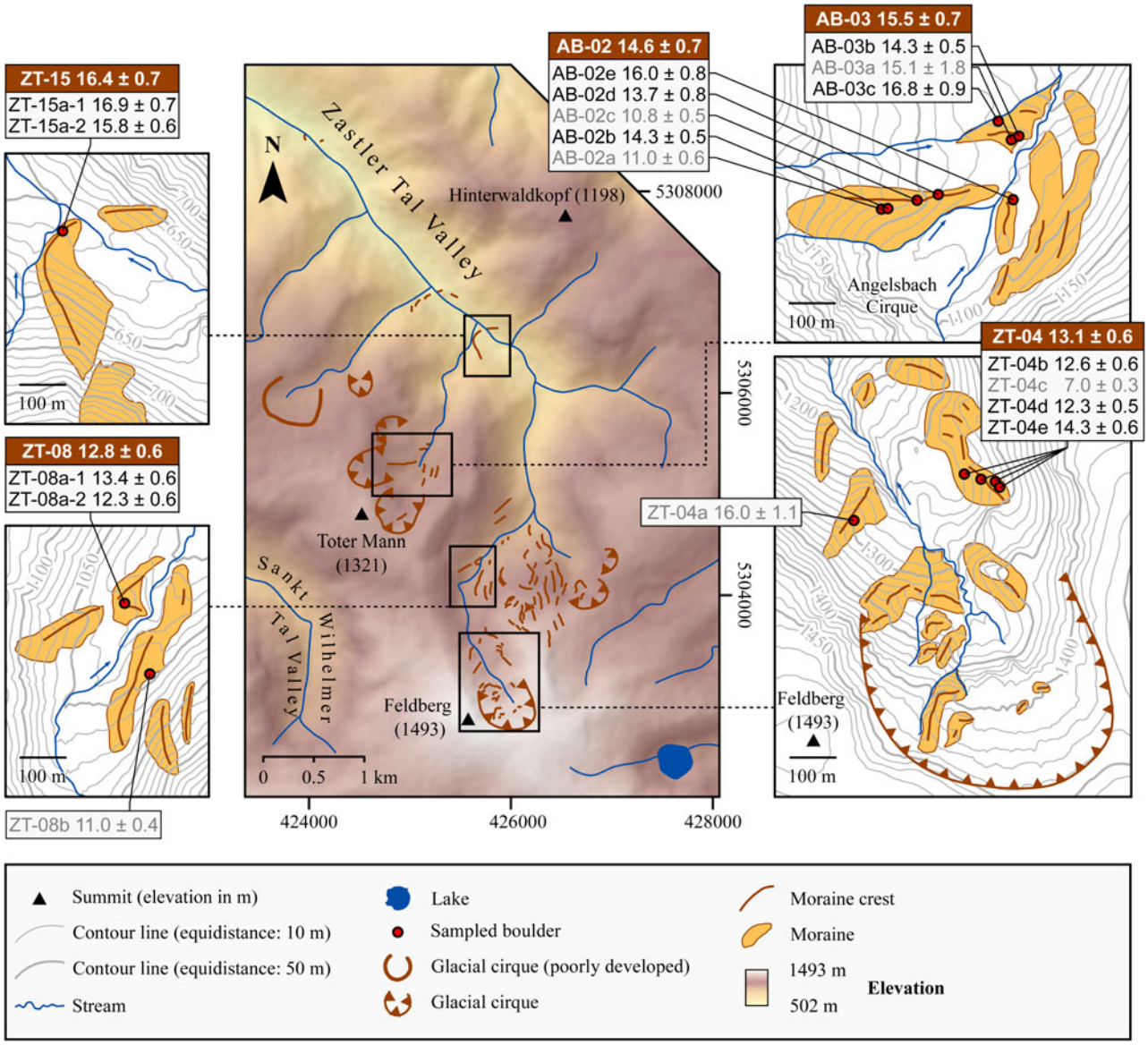

Figure 6. Glacial landforms in the Zastler Tal Valley (Hofmann et al., 2020) and boulders sampled for CRE dating. Exposure ages of moraine boulders and external uncertainties are given in ka (kiloyears before 2010 CE and ka, respectively). Ages in white font (brown boxes) are landform ages. Individual ages are presented in gray boxes. Ages in gray font were excluded (see the text for explanation). The source of the DEM is given in caption of Figure 2.

moraine on the valley floor farther upvalley (at ice-marginal position ZT-16) had large and stable boulders on its west-southwest facing side. However, this part of the moraine probably was partly removed by a nearby stream, therefore these boulders may have been reworked and were not sampled. Only one well-rounded and large boulder on a moraine at ice-marginal position ZT-15 proved to be a suitable candidate for exposure dating. Two sampling surfaces on the boulder, ZT-15a-1 and ZT-15a-2, gave exposure ages of 16.9 ± 0.7 ka and 15.8 ± 0.6 ka, respectively, resulting in a mean age of 16.4 ± 0.7 ka.

No suitable boulders were observed on moraines at ice-marginal positions ZT-14 to ZT-10. Two sampling surfaces (ZT-08a-1 and ZT-08a-2) on the ZT-08a boulder were exposure dated. This boulder was located on the double-crested moraine at ice-marginal positions ZT-09 and ZT-08. The ZT-08a-1 and ZT-08a-2 sampling surfaces gave ages of 13.4 ± 0.6 ka and 12.3 ± 0.6 ka, respectively. The ZT-08b boulder farther southeast gave an exposure age of 11.0 ± 0.4 ka. Because χ^2_R (8.8) was higher than the critical value, the age of the ZT-08b boulder was classified as an outlier. A landform age of 12.8 ± 0.6 ka was calculated for the moraine at ice-marginal position ZT-08. The moraines at ice-marginal positions ZT-07, ZT-06, and ZT-05 were devoid of sufficiently large and stable boulders.

Five boulders were sampled on two moraines at ice-marginal position ZT-04. The ZT-04a boulder on the westernmost moraine at this ice-marginal position was exposure dated to 16.0 ± 1.1 ka. The ZT-04b, ZT-04c, ZT-04d, and ZT-04e boulders on a moraine farther east gave exposure ages of 12.6 ± 0.6 ka, 7.0 ± 0.3 ka, 12.3 ± 0.5 ka, and 14.3 ± 0.6 ka, respectively. ^{9}Be currents dropped from 1.6 µA to 0.3 µA during AMS measurements on the ZT-04a sample, thus the age of the ZT-04a boulder was considered unreliable and excluded from further analysis. The age of the ZT-04c boulder (7.0 ± 0.3 ka) was classified as an outlier. Averaging the remaining ages resulted in a landform age of

https://doi.org/10.1017/qua.2023.53 Published online by Cambridge University Press

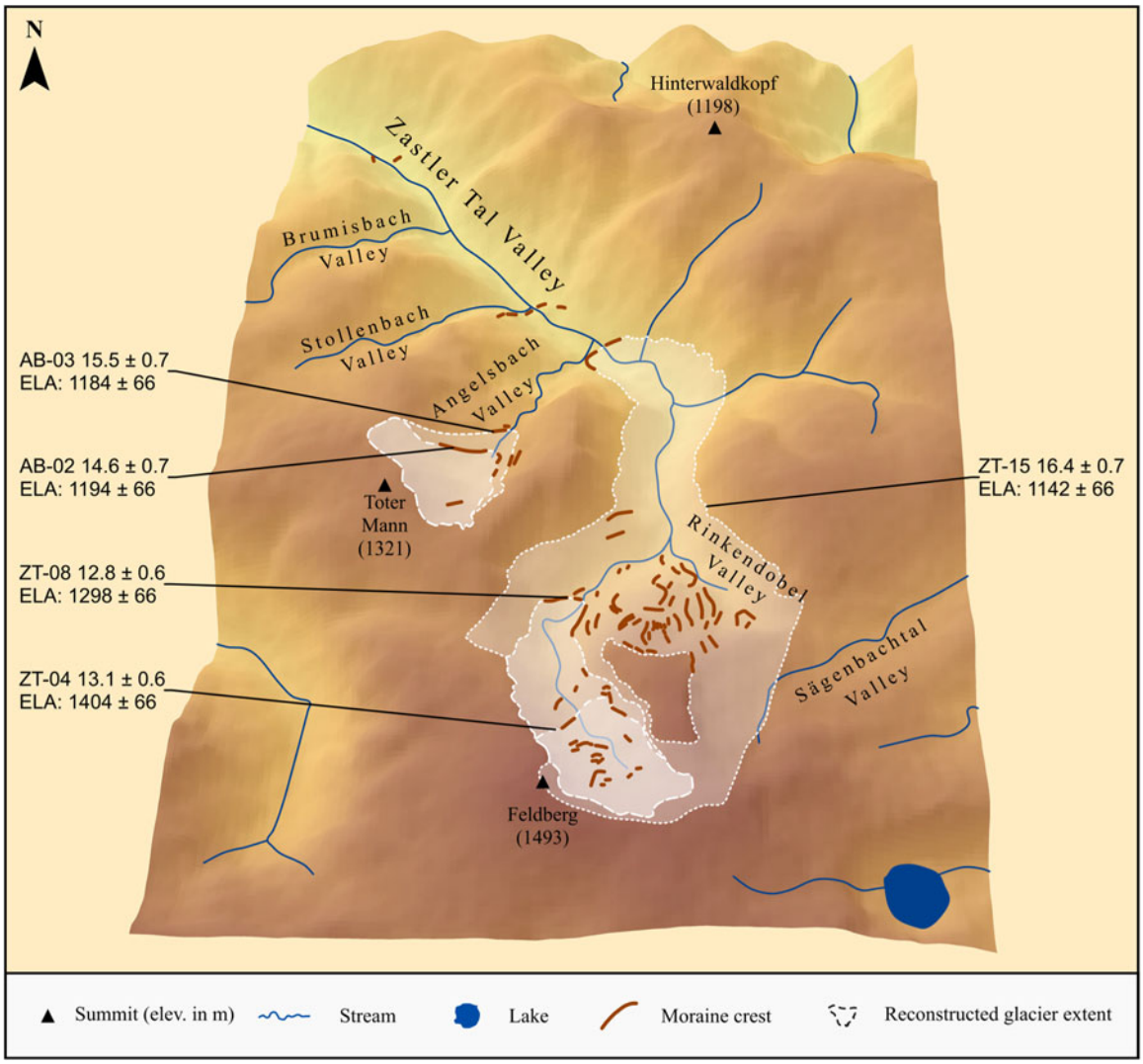

Figure 7. Moraine record in the Zastler Tal Valley and reconstructed glacier extents. CRE ages and associated external uncertainties are presented in ka. ELAs are given in m. See Figure 2 for the data source of the DEM.

13.1 ± 0.6 ka. No suitable boulders were identified on the moraines in younger morphostratigraphic positions (ice-marginal positions ZT-03, ZT-02, and ZT-01).

The moraine at ice-marginal position AB-05 in the Angelsbach Cirque was devoid of suitable boulders for dating. Three boulders, AB-03a, AB-03b, and AB-03c, were sampled on the double-crested moraine at ice-marginal positions AB-04 and AB-03 and gave exposure ages of 15.1 ± 1.8 ka, 14.3 ± 0.5 ka, and 16.8 ± 0.9 ka, respectively. Due to a sharp decline of ^{9}Be currents (from 3.8 µA to 0.2 µA) during AMS measurements on the AB-03a sample, the age was not considered reliable and excluded. Averaging the remaining two ages resulted in a landform age of 15.5 ± 0.7 ka.

Five boulders on two moraines at ice-marginal position AB-02 met the criteria for sampling. The AB-02a, AB-02b, AB-02c, and AB-02d boulders on a large ice-marginal moraine on the left-hand side of the former glacier yielded exposure ages of 11.0 ± 0.6 ka, 14.3 ± 0.5 ka, 10.8 ± 0.5 ka, and 13.7 ± 0.8 ka, respectively. The largest boulder sampled in the entire study area

Table 3. Ages of moraines in the Angelsbach Cirque and in the Zastler Tal Valley. χ^2_R was computed as outlined in Balco (2011).

Locality	Ice-marginal position	Number of CRE ages (outliers)	Landform age and uncertainty (ka) after the exclusion of outliers	χ^2_R
Angelsbach Cirque (AB)	AB-02	5 (2)	14.6 ± 0.7	16.6
	AB-03	3 (1)	15.5 ± 0.7	12.0
Zastler Tal Valley (ZT)	ZT-04	5 (2)	13.1 ± 0.6	98.4
	ZT-08	3 (1)	12.8 ± 0.6	8.8
	ZT-15	2 (0)	16.4 ± 0.7	—

https://doi.org/10.1017/qua.2023.53 Published online by Cambridge University Press

(AB-02e) on a moraine farther east gave an age of 16.0 ± 0.8 ka. χ^2_R considerably exceeded the critical value, therefore the ages of the AB-02a and AB-02c boulders were excluded. Averaging the remaining ages resulted in a landform age of 14.6 ± 0.7 ka.

The moraine at ice-marginal position AB-01 was devoid of boulders suited for CRE dating.

Reconstructed glaciers and ELAs

ELAs are presented in Table 4 and Figure 7, with the latter also displaying reconstructed glacier extents.

For the moraines at ice-marginal position ZT-15, an ELA of 1142 ± 66 m was determined. The moraines at ice-marginal position ZT-08 formed in front of a small valley glacier in the upper reaches of the Zastler Tal Valley. The equilibrium-line of this glacier was situated at 1298 ± 66 m. An ELA of 1400 ± 66 m was inferred for the moraines at ice-marginal position ZT-04. During moraine formation, glaciation of the valley was restricted to the stairway cirque in the uppermost part of the valley. The moraines at ice-marginal positions AB-03 and AB-02 probably formed at the margin of a cirque glacier. An ELA of 1184 ± 66 m was reconstructed for ice-marginal position AB-03. During formation of the moraines at ice-marginal position AB-02, the ELA was not considerably different (1194 ± 66 m).

Annual precipitation at ELAs

The reconstructed annual precipitation at the ELAs during moraine formation is presented in Table 5. At the onset of glacier recession from the moraine at ice-marginal position ZT-15, annual precipitation at the ELA was 920–2420 mm/yr. The reconstructed annual precipitation thus was indistinguishable from the average annual precipitation in the area around the former ELA during the period 1961–1990 CE (1700 mm/yr). We observed a similar pattern for ice-marginal positions AB-03 and AB-02 (1030–2540 mm /yr and 1330–2860 mm/yr, respectively), the reconstructed annual precipitation at the ELA had a similar order of magnitude as the average annual precipitation during the period 1961–1990 CE (1760 mm/yr). Due to the large uncertainty of the P/T function (standard error = 648 mm/yr) used to reconstruct precipitation, annual precipitation might have been considerably lower or higher than during the 1961–1990 CE period.

Potential snow-blow and avalanche areas

Snow-blow factors, avalanche ratios, and avalanche and snow-blow ratios are given in Table 6. See Figure 8 for reconstructed avalanche and snow-blow areas for ice-marginal positions in the Sankt Wilhelmer Tal Valley and in the Zastler Tal Valley. Figure 9B shows that avalanche ratios do not explain the observed variations in ELAs. Plotting snow-blow factors against ELAs and performing linear regression showed a strong negative relationship between these variables (Fig. 9C); snow-blow factors account for 69% of the variation in ELAs ($p < 0.05$). We observed a stronger negative relationship between the snow-blow/avalanche ratios and ELAs:

$$ELA = -44.53 \times r_{s,a} + 1261.35$$

where $r_{s,a}$ is the snow-blow/avalanche ratio. Of the variance in ELA values, 80% is attributable to differences in snow-blow/avalanche

Table 4. Landform ages, associated uncertainties, and ELAs for moraines in the Zastler Tal Valley and in the Sankt Wilhelmer Tal Valley.

Locality		Ice-marginal position	CRE age and internal uncertainty in ka (external uncertainty in parentheses)	ELA (m)	Reference
Zastler Tal Valley	Main valley	ZT-04	13.1 ± 0.5 (0.6)	1400 ± 66	This study
		ZT-08	12.8 ± 0.5 (0.6)	1298 ± 66	
		ZT-15	16.4 ± 0.5 (0.7)	1142 ± 66	
	Angelsbach Cirque	AB-02	14.6 ± 0.6 (0.7)	1194 ± 66	
		AB-03	15.5 ± 0.6 (0.7)	1184 ± 66	
Sankt Wilhelmer Tal Valley	Main valley	SW-02 and SW-03	14.0 ± 0.8 (0.8)	1195 ± 66	Hofmann et al. (2022)
		SW-09	16.1 ± 0.6 (0.7)	1132 ± 66	
		SW-10	16.0 ± 0.8 (0.9)	1132 ± 66	
		SW-11	17.5 ± 0.9 (1.0)	1123 ± 66	
		SW-12	17.0 ± 0.6 (0.7)	1123 ± 66	
		SW-15	17.0 ± 0.6 (0.7)	—	
		SW-17	16.3 ± 0.6 (0.7)	—	
		SW-18	17.2 ± 0.7 (0.8)	—	
	Katzensteig Cirque	KS-01	14.3 ± 0.5 (0.6)	1147 ± 66	
		KS-02	14.2 ± 0.6 (0.7)	1143 ± 66	
		KS-03	14.0 ± 0.6 (0.7)	1143 ± 66	
	Wittenbach Cirque	WB-01	ca. 14 (?)	1201 ± 66	
		WB-02	ca. 14 (?)	1194 ± 66	
		WB-03	ca. 14 (?)	1178 ± 66	

https://doi.org/10.1017/qua.2023.53 Published online by Cambridge University Press

Table 5. Reconstructed annual precipitation for ice-marginal positions AB-02, AB-03, and ZT-15.

Ice-marginal position	ELA (m)	T_{July} at Burgäschisee (°C)	T_{July} at the ELA (°C)	T_3 at the ELA (°C)	P_a at the ELA (mm/yr)	Current P_a (mm/yr)
AB-02	1194 ± 66	10.5 ± 1.4	5.8 ± 1.4	4.4 ± 1.4	1330–2860	1760
AB-03	1184 ± 66	9.3 ± 1.4	4.6 ± 1.4	3.3 ± 1.4	1030–2540	1760
ZT-15	1142 ± 66	8.6 ± 1.4	4.2 ± 1.4	2.9 ± 1.4	920–2420	1700

Table 6. ELAs, potential snow blow, avalanche, and snow-blow/avalanche areas for ice-marginal positions in the Zastler Tal Valley and in the Sankt Wilhelmer Tal Valley.

Ice-marginal position	ELA (m)	Glacier area (km^2)	Potential snow-blow area (km^2)	Snow-blow factor	Potential avalanche area (km^2)	Avalanche ratio	Potential snow-blow & avalanche area (km^2)	Avalanche and snow-blow ratio
AB-02	1194 ± 66	0.39	0.62	1.26	0.03	0.09	0.65	1.66
KS-01	1147 ± 66	0.41	1.08	1.62	0.05	0.12	1.11	2.71
KS-02 & KS-03	1143 ± 66	0.52	1.22	1.53	0.03	0.06	1.23	2.36
SW-02 & SW-03	1195 ± 66	1.53	1.46	0.98	0.68	0.45	2.08	1.36
WB-01	1201 ± 66	0.86	1.34	1.25	0.09	0.11	1.42	1.66
WB-02	1194 ± 66	0.91	1.42	1.25	0.14	0.15	1.53	1.68
WB-03	1178 ± 66	1.06	1.49	1.19	0.20	0.19	1.66	1.57

ratios ($p < 0.05$; Fig. 9D). Figure 9D shows that clustering of data points may indicate a strengthened relationship between snow-blow/avalanche ratios and ELAs. To further assess the relationship between the two variables, ELAs, potential snow-blow areas, and potential avalanche areas of other glaciers in the Southern Black Forest need to be reconstructed. Since the regression line intercepts the ordinate at ~1260 m, a hypothetical glacier without snow-blow and avalanching catchments would have had an ELA of this elevation.

DISCUSSION

Deglaciation chronology

Due to the lack of suitable boulders, the onset of glacier retreat from the presumably oldest ice-marginal positions (ZT-18, ZT-17, and ZT-16) could not be determined. We were unable to verify the previous assumption (Erb, 1948; Liehl, 1982; Metz and Saurer, 2012) that these moraines are of Late Pleistocene age and that the moraine at ice-marginal position ZT-18 documents the Late Pleistocene maximum ice extent. We argue that the dated moraine at ice-marginal position ZT-15 should be regarded as a recessional moraine due to its limited size. Thus, the timing of glacier retreat from the presumed Late Pleistocene maximum position remains unknown for the time being. Glacier recession from the moraine at ice-marginal position ZT-15 was underway by 16.4 ± 0.7 ka at the latest. The Angelsbach Cirque glacier withdrew from ice-marginal positions AB-03 and AB-02 no later than 15.5 ± 0.7 and 14.6 ± 0.7 ka, respectively. The Zastler glacier receded from the moraines at ice-marginal position ZT-08 no later than 12.8 ± 0.6 ka. Because the sampling surfaces on the flat ZT-08a boulder were not situated high above ground, they might have weathered out of the moraine well after glacier retreat. Glacier retreat probably occurred earlier than suggested by the CRE ages. Glacier recession from ice-marginal position ZT-04 occurred by 13.1 ± 0.6 ka at the latest.

Figures 10 and 11 show a compilation of previously published ^{10}Be CRE ages for the Southern Black Forest (Hofmann et al., 2022) and chronological data obtained for this study (see also Table 4). Because we only refer to ^{10}Be CRE ages in this subsection, both internal and external uncertainties are given, the latter in brackets. Within the temporal resolution of CRE dating, it appears that the valley glaciers receded simultaneously from the moraines at ice-marginal positions ZT-15 (16.4 ± 0.5 [0.7] ka) and SW-09 (16.1 ± 0.6 [0.7] ka) in the Zastler Tal Valley and the Sankt Wilhelmer Tal Valley, respectively. Glacier retreat from the moraine at ice-marginal position AB-02 (no later than 14.6 ± 0.6 [0.7] ka) may have occurred simultaneously with glacier recession from the moraine at ice-marginal positions SW-03 and SW-02 in the Sankt Wilhelmer Tal Valley (by 14.0 ± 0.8 [0.8] ka at the latest), and from the moraines at ice-marginal positions KS-03, KS-02, and KS-01 in the Katzensteig Cirque (no later than 14.0 ± 0.6 [0.7] ka, 14.2 ± 0.6 [0.7] ka, and 14.3 ± 0.5 [0.6] ka, respectively). As outlined previously, the moraines at ice-marginal positions WB-01 to WB-03 in the Wittenbach Cirque lie in similar morphostratigraphic positions to those at ice-marginal positions AB-02, KS-01 to KS-03, SW-02, and SW-03. Therefore, these moraines are probably of a similar age. We propose that a common forcing led to glacier retreat in the Angelsbach, Katzensteig, and Wittenbach Cirques, as well as in the cirque in the upper reaches of the Sankt Wilhelmer Tal Valley senso strictu. The minimum age for the onset of glacier recession overlap with the rapid warming in summer temperatures is ca. 14.7 ka (Heiri et al., 2014a). Therefore, it is possible that this abrupt rise in summer temperatures might have driven glacier retreat.

The uncorrected CRE ages of ice-marginal positions ZT-04 (13.1 ± 0.6 ka) and ZT-08 (12.8 ± 0.6 ka) overlap with the cool phase in Central Europe of 12.9–11.7 ka, documented elsewhere (cf., Heiri et al., 2014a). However, correcting these landform ages for postglacial denudation and snow shielding leads to

https://doi.org/10.1017/qua.2023.53 Published online by Cambridge University Press

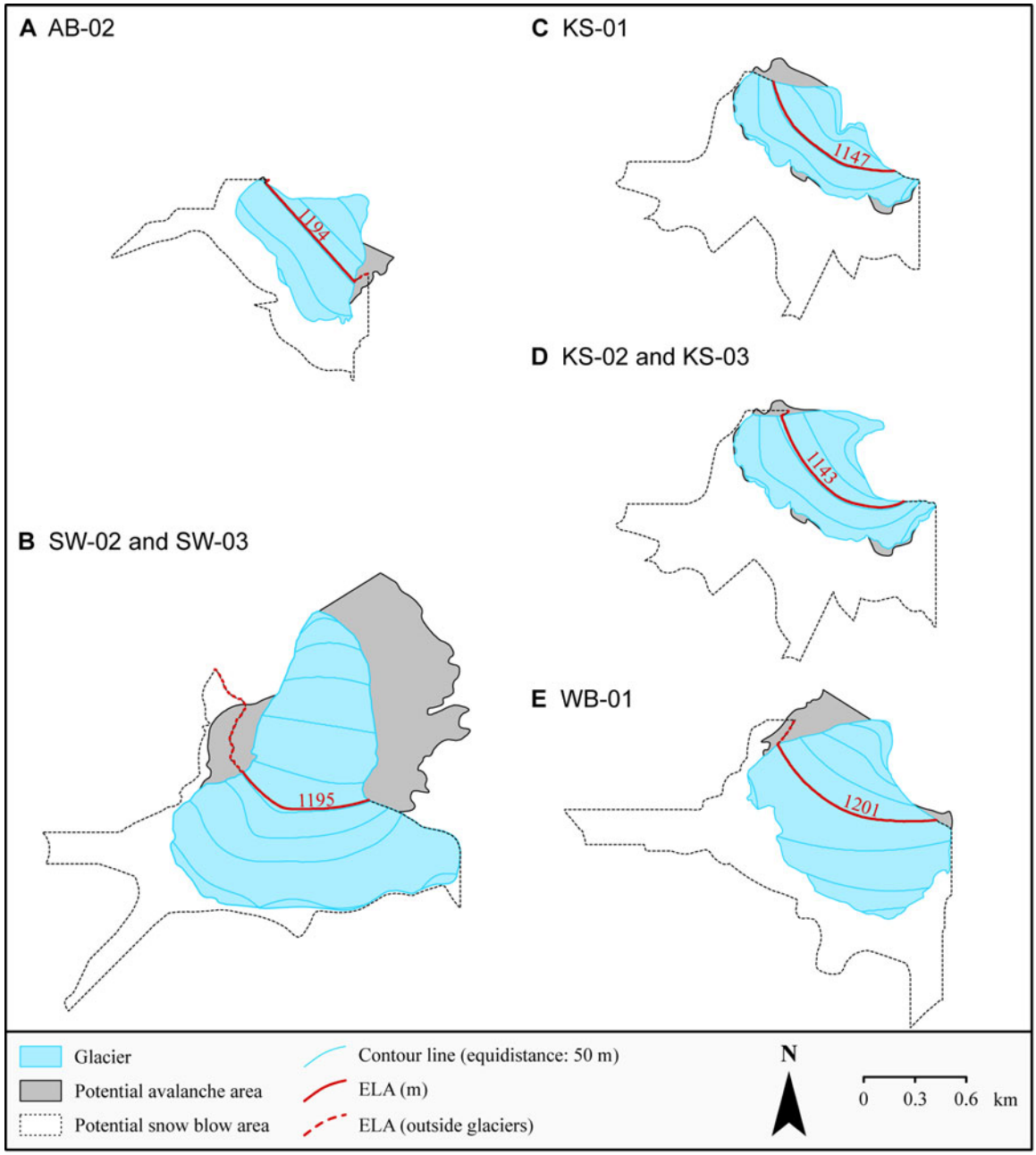

Figure 8. Potential avalanche and snow-blow areas for selected ice-marginal positions. (**A**) AB-02, (**B**) SW-02 and SW-03 (**C**) KS-01, (**D**) KS-02 and KS-03, (**E**) WB-01.

landform ages of ca. 13.8 ± 0.6 ka (ZT-04) and 13.6 ± 0.7 ka (ZT-08), which predate the cool phase. Possibly, these ice-marginal positions could be linked with decadal to centennial cooling events at ca. 14 ka, ca. 13.5 ka, or ca. 12.9 ka, respectively (cf., Heiri et al., 2014a).

Spatial discrepancies in ELAs and their causes

In Figure 12, ELAs for ice-marginal positions are color-coded according to their CRE ages. ELAs for ice-marginal positions with a CRE age of 17–16 ka, 15–14 ka, and 13 ka are shown in yellow, orange, and dark red, respectively. ELAs were similar in the Zastler Tal Valley and in the Sankt Wilhelmer Tal Valley in the 17–16 ka period. ELAs between 1123 ± 66 m and 1142 ± 66 m were reconstructed for ice-marginal positions ZT-15, SW-09, SW-10, SW-11, and SW-12. Calculating ELAs for the ice-marginal positions with a CRE age of about 15–14 ka (i.e., for ice-marginal position AB-02 in the Zastler Tal Valley and ice-marginal positions SW-02, SW-03, KS-01, KS-02, and KS-03 in the Sankt Wilhelmer Tal Valley) resulted in a strong scatter. ELAs range from 1143 ± 66 m to 1194 ± 66 m. As shown previously, 80% of the variance in ELAs at around 15–14 ka is attributable to differences in avalanche/snow-blow ratios. This suggests that the observed variation in ELAs at 15–14 ka results from topoclimatic factors, namely snow blow and avalanching. High avalanche/snow-blow ratios for ice-marginal positions KS-01 to KS-03 support the assumption that the Katzensteig Cirque glacier owed its existence to a relatively large snow-contributing area.

https://doi.org/10.1017/qua.2023.53 Published online by Cambridge University Press

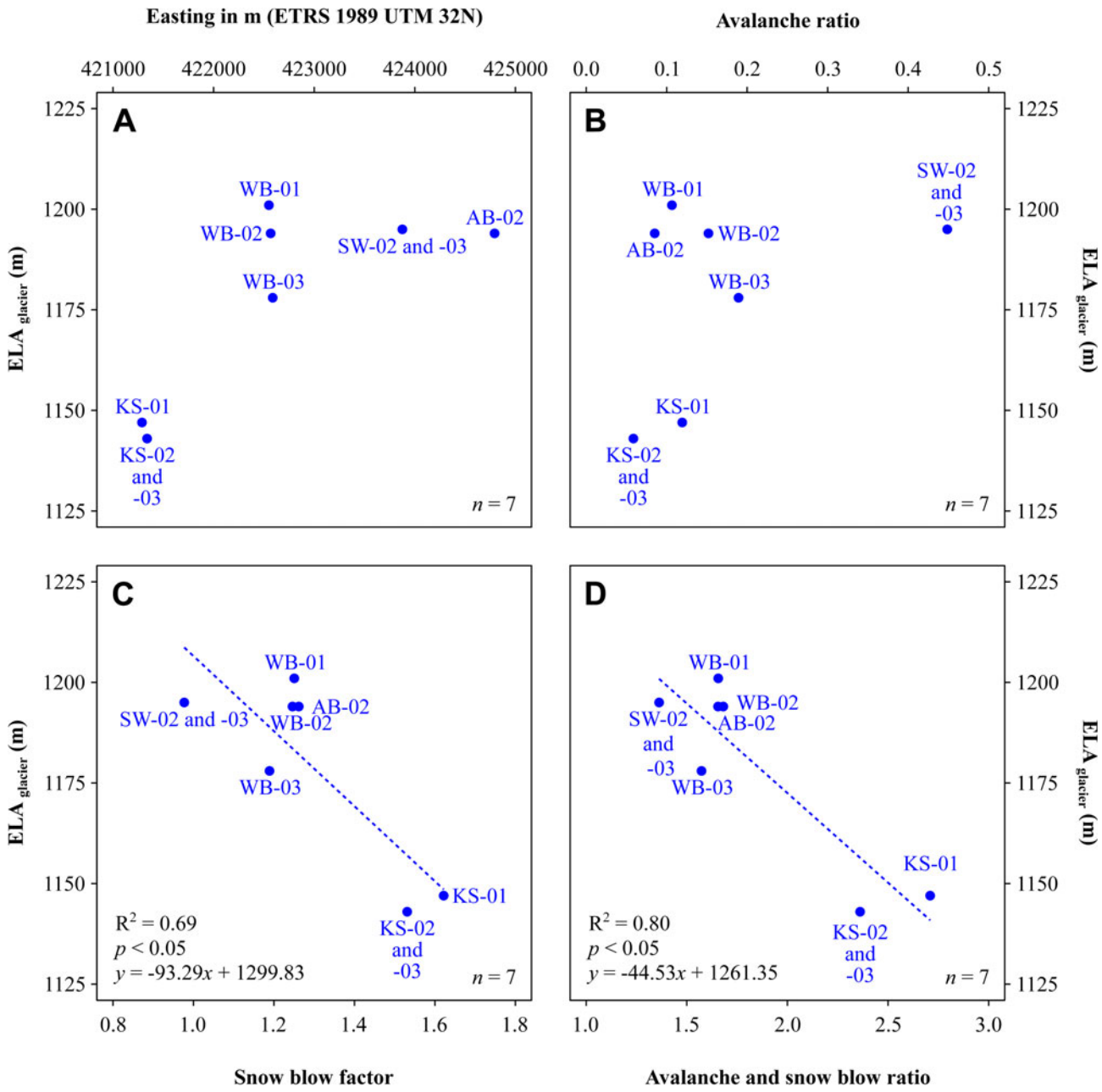

Figure 9. (**A**) *y*-coordinates of midpoints of ELAs (UTM coordinate system) in the Zastler Tal Valley and in the Sankt Wilhelmer Tal Valley versus ELAs (in meters) of glaciers $ELA_{glacier}$ (m). (**B**) Avalanche ratios versus $ELA_{glacier}$. (**C**) Snow-blow factors versus $ELA_{glacier}$. (**D**) Avalanche and snow-blow ratios versus $ELA_{glacier}$.

Are the ELA-based estimates of annual precipitation realistic?

The few available precipitation records for the last glacial termination imply that annual precipitation in the southern part of Central Europe was significantly lower than today (Guiot et al., 1989; Peyron et al., 2005; Magny et al., 2006), particularly before the increase in summer temperatures at ca. 14.7 ka (cf., Peyron et al., 2005; Magny et al., 2006). A pollen-based reconstruction revealed that annual precipitation at Lac Lautret in the Jura (Fig. 1) amounted to about 350 mm/yr before the rapid rise in summer temperatures in Central Europe at ca. 14.7 ka (Peyron et al., 2005; Magny et al., 2006). Annual precipitation was thus considerably lower than present-day precipitation (~1500 mm/yr; Magny et al., 2006). According to Guiot et al. (1989), annual precipitation at the Grande Pile Bog in the southwestern part of the Vosges (Fig. 1) amounted to less than 20% of current average annual precipitation (~1000 mm/yr; Ponel, 1995) prior to 14 ka. The lower bounds of reconstructed annual precipitation for ice-marginal positions ZT-15, AB-03, and AB-02 (920, 1030, and 1330 mm/yr) concur with the common hypothesis of low precipitation in Central Europe during the last glacial termination. However, due to the large uncertainties of the precipitation reconstructions that predominantly result from the large error of the used P/T function (standard error = 648 mm/yr; Ohmura and Boettcher, 2018), we cannot exclude the scenario that annual precipitation at the ELA at 17–16 ka and around 15–14 ka was equal to average annual precipitation in the 1961–1990 CE period or even exceeded present-day precipitation.

https://doi.org/10.1017/qua.2023.53 Published online by Cambridge University Press

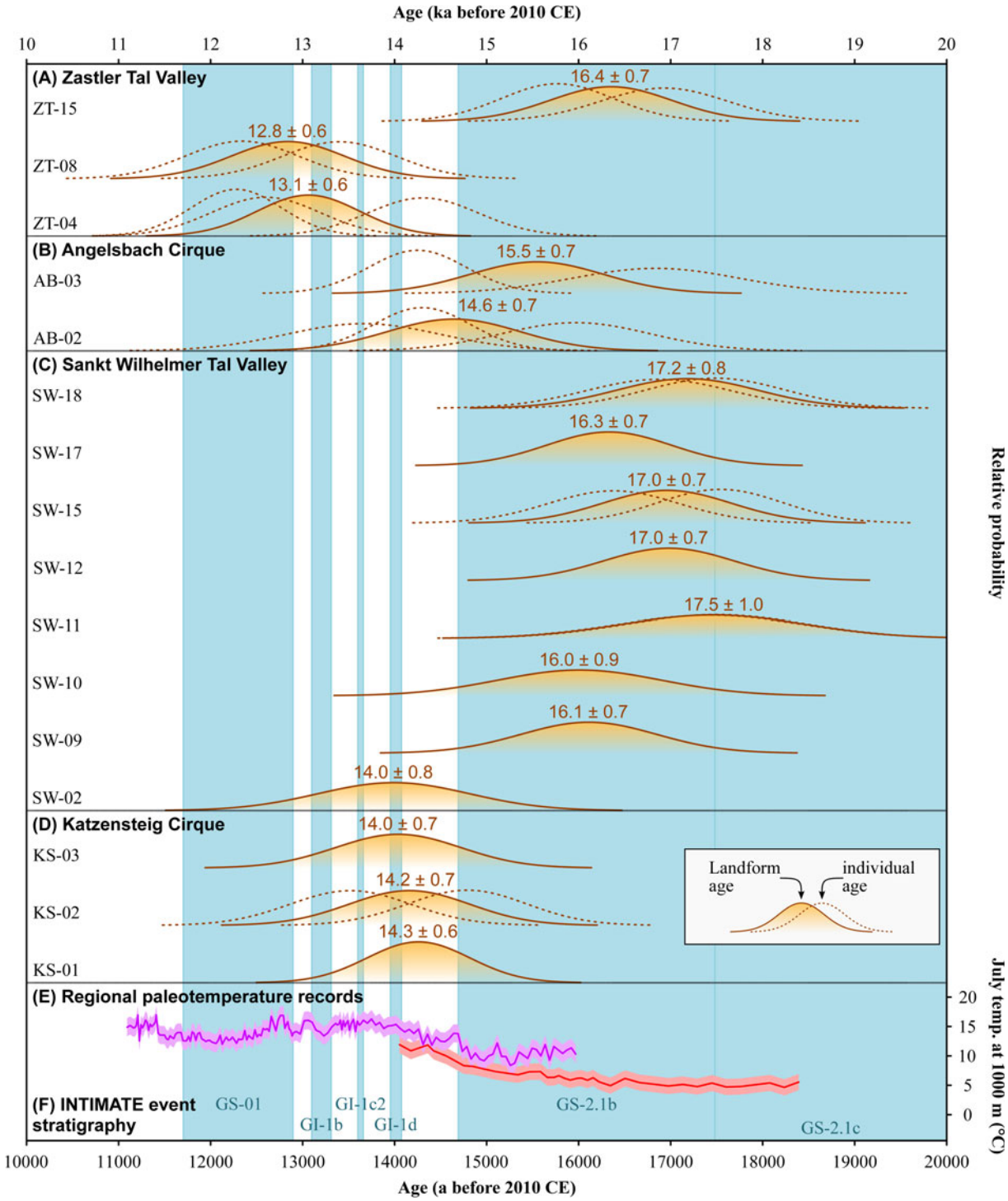

Figure 10. Probability density functions of periods of glacier recession from ice-marginal positions in the (**A**) Zastler Tal Valley (this study), (**B**) Angelsbach Cirque (this study), (**C**) Sankt Wilhelmer Tal Valley (Hofmann et al., 2022), and (**D**) Katzensteig Cirque (Hofmann et al., 2022) according to CRE ages of moraines. (**E**) July temperature at 1000 m in the Southern Black Forest according to regional paleoclimate records. Chironomid-inferred July temperatures at Burgäschisee (Fig. 1) on the Swiss Plateau (red line; Bolland et al., 2020) and at Lac Lautrey (Fig. 1) in the French Jura (purple line; Heiri and Millet, 2005) were adjusted to an elevation of 1000 m, assuming a lapse rate of 7 °C/km (Kuttler, 2013). (**F**) Greenland stadials (GS) and interstadials (GI) according to the INTIMATE event stratigraphy (Rasmussen et al., 2014) are shown for comparison.

To answer the question whether actual annual precipitation at the ELAs was closer to the upper or lower bounds of the precipitation estimates, an in-depth discussion of the limitations of the ELA-based precipitation reconstruction is mandatory. A detailed assessment of the aforementioned studies on annual precipitation during the last glacial termination is beyond the scope of this paper. In the following sub-sections, we discuss limitations of the methodology adopted for this study, including (1) uncertainties of reconstructed glacier surfaces, (2) robustness of the reconstructed ELAs, (3) uncertainties of CRE ages of ice-marginal

https://doi.org/10.1017/qua.2023.53 Published online by Cambridge University Press

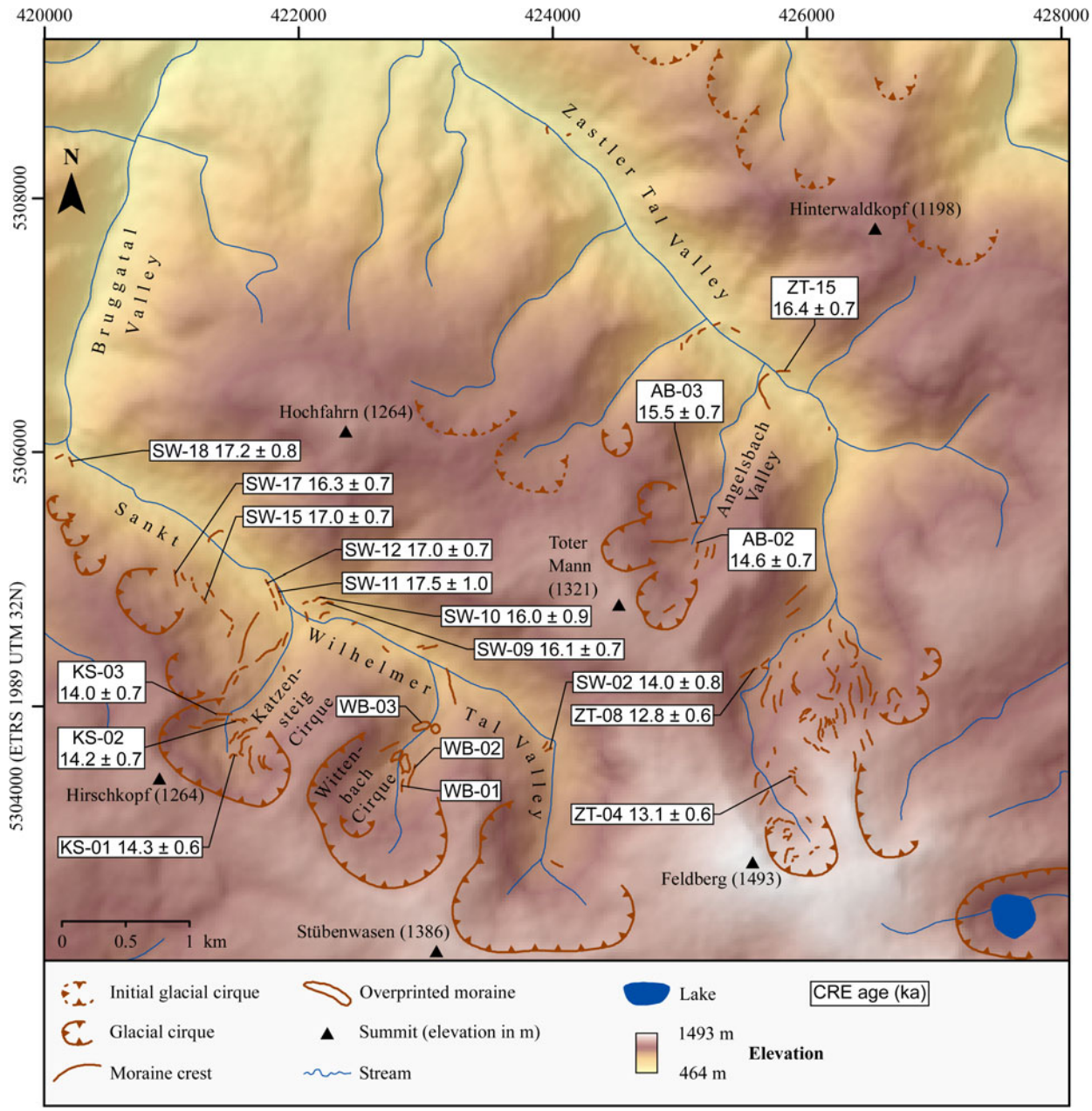

Figure 11. Glacial landforms in the Sankt Wilhelmer Tal Valley, Zastler Tal Valley, and in the surrounding region (Hofmann et al., 2020, 2022). Landform ages in white boxes are given in ka before 2010 CE. See Figure 2 for the data source of the shaded relief.

positions, and (4) the reliability of the July temperature record used. We also consider (5) shortcomings of the P/T function, and (6) the potential role of factors other than precipitation and temperature that may have influenced the mass balance of the reconstructed glaciers.

Uncertainties of reconstructed glacier surfaces

The range of published shear stress values beneath modern glaciers is large (e.g., Paterson, 1970; Boulton et al., 1979; Cohen, 2005) and, therefore, the choice of this value is regarded as the major source of uncertainty in glacier surface reconstructions. The reconstruction of glacier geometry during moraine formation was not straightforward for all ice-marginal positions. While ice-marginal positions ZT-08, ZT-04, AB-03, and AB-02 are well documented by moraines and the upper limits of the headwall of cirques, ice-marginal position ZT-15 is only represented by two moraines near the former glacier terminus. It follows that the ELA for ice-marginal positions ZT-08, ZT-04, AB-03, and AB-02 should be considered much more reliable than the ELA for ice-marginal position ZT-15. Because the Angelsbach Cirque glacier was small during emplacement of the moraines at ice-marginal positions AB-03 and AB-02, and the former glacier extent is well documented by geomorphological evidence, we argue that the glacier surface reconstruction likely introduced only a small error to the precipitation estimates.

Robustness of the reconstructed ELAs

For ELA reconstructions, we chose the (median) global AABR (1.56) presented by Oien et al. (2022). It should be noted that this balance ratio was derived from glaciers across the globe in

https://doi.org/10.1017/qua.2023.53 Published online by Cambridge University Press

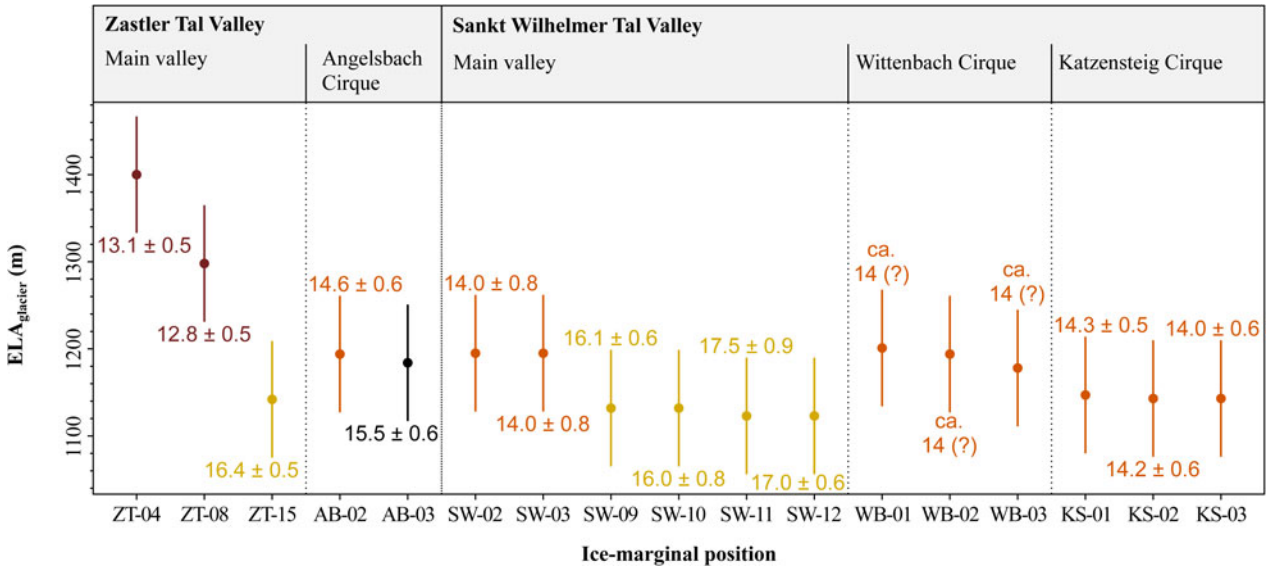

Figure 12. Reconstructed ELAs for ice-marginal positions in the Zastler Tal Valley sensu stricto, in the Angelsbach Cirque, as well as recalculated ELAs for ice-marginal positions in the Sankt Wilhelmer Tal Valley sensu stricto, in the Wittenbach Cirque, and in the Katzensteig Cirque (Hofmann et al., 2022). See Figure 11 for the locations of the sites. CRE ages and associated internal uncertainties are given in ka.

various climatic settings, including areas with maritime and continental climates. Oien et al. (2022) also presented balance ratios for distinct regions of the world, such as the Alps, and demonstrated that use of the balance ratio for this region allowed for reducing the discrepancy between calculated and actual ELAs of the considered glaciers from ~110 m to ~70 m. Hofmann et al. (2022) argued that glaciers in the Alps are probably the best analogues for the former glaciers in the study area. It is conceivable that use of the balance ratio for the Alps could have resulted in more appropriate AABR–ELAs. If we had chosen the balance ratio for the Alps for ELA calculations, we would have needed to select a specific precipitation/temperature function for the Alps to ensure consistency. Following the recommendation of Golledge et al. (2010), who advocated the use of regional precipitation/temperature functions, we extracted data on annual precipitation and summer temperature at the ELAs of 16 glaciers in the Alps from the dataset of Ohmura and Boettcher (2018). We subsequently plotted summer temperature versus annual precipitation at the ELA and performed a linear regression. This analysis revealed the absence of a clear relationship between these variables ($R^2 = 0.00$; $p = 0.88$). It follows that a specific precipitation/temperature function for the Alps cannot be established with the data from Ohmura and Boettcher (2018). Therefore, we argue that the approach selected for this study (i.e., the application of the [median] global AABR and use of the precipitation/temperature function of Ohmura and Boettcher, 2018) remains the most robust approach for precipitation reconstruction. The methodology is consistent with the recommendation of Oien et al. (2022) who advocated the use of the median global AABR if "boundary conditions relevant to the mass-balance regime" (Oien et al., 2022, p. 366) are likely to have been different in the past. Oien et al. (2022) found that the median absolute difference between actual ELAs of glaciers around the globe ($n = 64$) and those determined with the global median AABR of glaciers amounted to 65.5 m. Assuming a lapse rate of 6.5°C/km (ISO 2533:1975; https://www.iso.org/standard/7472.html), we infer that the uncertainty of the AABR method introduces an error of 0.42°C in the summer temperature at the ELA. This compares favorably with the uncertainty of the utilized July temperature record (~1.4°C).

Uncertainties of CRE ages of ice-marginal positions

For the precipitation reconstruction, we assumed that uncorrected landform ages indicate the timing of the onset of glacier recession from ice-marginal positions. Correcting the ages of ice-marginal positions for snow cover and postglacial denudation would lead to an increase of the ages in the order of 5%. If we had assumed that corrected ages were more appropriate, precipitation reconstructions would have yielded lower precipitation at the ELAs. For example, if we had used the corrected landform age (15.5 ± 0.8 ka) for ice-marginal position AB-02, we would have assumed a mean summer temperature at the ELA of 3.3 ± 1.4°C instead of 4.4 ± 1.4°C, which would have resulted in lower annual precipitation at the ELA (1030–2530 mm/yr instead of 1330–2860 mm yr). This reasoning supports the hypothesis that the lower bounds of the estimates of annual precipitation should be regarded as the most realistic.

Reliability of the July temperature record used

For the reconstruction of annual precipitation at the ELA, a July temperature record based on chironomid assemblages was used. It has been suggested that chironomids also react to environmental variables other than peak summer temperatures, such as seasonality (cf., Eggermont and Heiri, 2012; Schenk et al., 2018). It is therefore possible that the peak summer temperatures inferred by chironomid assemblages may have introduced a bias in the ELA-based precipitation reconstruction, but we cannot determine whether this bias led to an over- or underestimation of annual precipitation at the ELA. As outlined previously, the average July temperature at Burgäschisee was adjusted to the ELAs in the Southern Black Forest assuming a 6.5°C/km lapse rate. However, catabatic effects and the larger albedo of glacier surfaces lead to lower temperatures in areas adjacent to glaciers (cf., Golledge et al., 2010). Therefore, adjusting July temperatures

https://doi.org/10.1017/qua.2023.53 Published online by Cambridge University Press

from an ice-free environment (Burgäschisee) to ELAs in the study area probably led to an overestimation of July temperatures at the ELAs. To the best of our knowledge, no quantitative temperature reconstruction has been published for a site close to the glaciers of the Southern Black Forest. To improve the accuracy and reliability of glacier-based precipitation reconstructions, temperature reconstructions for mid-elevation mountainous regions in Central Europe would be beneficial but might be limited by a lack of suitable archives.

Shortcomings of the P/T function

Two shortcomings of the P/T function of Ohmura and Boettcher (2018) have to be considered when discussing the robustness of the estimates of annual precipitation. First, the selected P/T function does not take continentality into account. The choice of this function might have led to a considerable overestimation of annual precipitation. This view is reinforced by ELA-based paleoprecipitation estimates for different regions around Scotland with a similar P/T function (Ohmura et al., 1992). The application of this function led to an overestimation of annual precipitation in the 12.9–11.7 ka cool period by more than 500 mm/yr (Golledge et al., 2010). Therefore, Braithwaite (2008, p. 442) argued that "users of exponential or power-law relations between accumulation and summer temperature should be prepared to calculate different curves to use in different climatic regions". Following this suggestion, Golledge et al. (2010) designed a specific P/T function for the 12.9–11.7 ka cool period in Scotland. Although these authors argued that continentality in Central Europe was less pronounced than in Scotland, it would be desirable to replace the P/T function of Ohmura and Boettcher (2018) by a more suitable one. Second, the standard error (648 mm/yr) of the P/T function is very large. Future studies should aim to develop a P/T function that allows for obtaining more precise estimates of annual precipitation at ELAs.

Potential role of factors other than precipitation and temperature that may have influenced mass balance of reconstructed glaciers

Reconstructed annual precipitation should be treated as "winter mass balance plus summer precipitation" (Hughes and Braithwaite, 2008, p. 113). There are several examples of glaciers that largely owe their existence to snow blow and avalanching, such as the small cirque glaciers in the Polar Urals in Russia. According to mass balance measurements (Voloshina, 1988) and data from a nearby weather station (Ananicheva and Kononov, written communication, 2007, in Mangerud et al., 2008), the winter mass balance of the Obruchev glacier was, on average, 5.3 times higher than winter precipitation from 1957–1962 CE (Mangerud et al., 2008). Winter mass balance of the IGAN glacier, the largest glacier in the Polar Urals, was, on average, 4.3 times higher than winter precipitation during the same period (Voloshina, 1988; Ananicheva and Kononov, written communication, 2007, in Mangerud et al., 2008). Although the estimated climatic ELA in the Polar Urals (~1600 m; Svendsen et al., 2023) might be overestimated (see discussion in Mangerud et al., 2008) and winter precipitation at the weather station might have been underestimated (Ivanov, 2012), the ELA of the Obruchev and IGAN glaciers was probably well below the climatic ELA from 1959–1962 CE (Voloshina, 1988). The annual temperature range (i.e., the difference between the mean temperature of the coldest month and the mean temperature of the warmest month) amounts to 30°C in the Polar Urals (Mangerud et al., 2008, Fig. 2). This is broadly equivalent to the temperature range in Central Europe during the last glacial termination (Isarin et al., 1998; Isarin and Renssen, 1999; Renssen and Isarin, 2001; Denton et al., 2005, 2010). Because the climatic setting in the Polar Urals resembles the climatic regime in Central Europe during the last glacial termination and since the glaciers in the Polar Urals are highly dependent on snow blow and avalanching, we argue that these ice masses might be good analogues for the former cirque glaciers in the Black Forest at around 15–14 ka. If we consider the possible scenario that annual precipitation only accounted for about one-fourth of the winter mass balance of the cirque glaciers in the Southern Black Forest, our estimate of annual precipitation at the ELA (or rather the winter mass balance plus summer precipitation), would largely exceed annual precipitation.

This raises the question of how we might correct the estimate of annual precipitation for the influence of snow blow and avalanching. As shown previously, a potential cirque glacier at 15–14 ka without a snow-blow and avalanche source area would have had a theoretical ELA of ~1260 m. We argue that inserting this theoretical ELA in the P/T function of Ohmura and Boettcher (2018) would not help us to tackle this issue because the mass balance of at least some glaciers in the dataset of Ohmura and Boettcher (2018) is affected by snow blow and/or avalanching. If we had used the theoretical ELA for precipitation reconstructions, we essentially would have corrected twice for snow blow and avalanching.

To revisit the question of whether the presented ELA-based estimates of annual precipitation are realistic, the considerations in the previous paragraphs lead to the conclusion that the lower bounds of the precipitation estimates are probably closest to actual annual precipitation at the ELAs. Reconstructing potential snow-contributing areas for cirque glaciers at 15–14 ka revealed that the mass balance of all considered glaciers was, at least to some extent, influenced by snow blow and avalanching. We therefore conclude that disentangling the contributions of snow blow/avalanching and annual precipitation, respectively, to the mass balance of small ice masses should be regarded as prerequisite for realistic estimates of annual precipitation at the ELA. This should be complemented by radiation modeling to assess the role of topographic shading on the mass balance of glaciers (e.g., Mills et al., 2012). It follows that further research is needed before ELAs of small ice masses, such as those in the Southern Black Forest, can be employed—if at all—for quantitative precipitation reconstructions.

CONCLUSIONS

This study provided valuable insights into the Late Pleistocene glaciation history of mid-elevation mountainous regions in Central Europe and complements the previously published first glacier chronology from the Southern Black Forest (Hofmann et al., 2022). Due to the lack of boulders suitable for CRE dating, the ages of the morphostratigraphically oldest moraines, hence, the onset of glacier retreat from the presumed Late Pleistocene maximum position, could not be determined. Periods of glacier recession from different ice-marginal positions during the subsequent deglaciation began no later than 16 ka, 15 ka, and 13 ka, respectively. Two phases of glacier retreat (no later than 16 ka and 15 ka, respectively) also are documented in the Sankt Wilhelmer Tal Valley southwest of the study area. This similarity supports the hypothesis that these phases of glacier recession were

https://doi.org/10.1017/qua.2023.53 Published online by Cambridge University Press

events of regional relevance. Assuming that these phases were climatically driven, the corresponding climatic shifts must have affected at least the Southern Black Forest.

The reconstructed annual precipitation at the ELAs at around 16 ka and 15–14 ka overlaps with the present-day precipitation but is associated with substantial uncertainties caused by the large error of the utilized P/T function. In addition, the following caveats should be considered when interpreting the ELA-based precipitation estimates: (1) extrapolating July temperatures from an ice-free region to a partly glaciated area may have led to overestimation of the summer temperature at the ELA, (2) the utilized P/T function does not adequately account for continentality, and (3) the ELAs of cirque glaciers at around 15–14 ka probably lay below the climatic ELA due to the influence of topoclimatic factors. Potential avalanche and snow-blow areas, and ELAs of additional glaciers at around 15–14 ka need to be reconstructed to assess the influence of topoclimatic factors in more detail. In addition, radiation modeling should be undertaken to assess the role of topographic shading. We conclude that the lower bounds of the precipitation estimates appear to be the most realistic. They concur with the common hypothesis that the amount of precipitation in the southern part of Central Europe was low at this time. Currently, the uncertainty of the P/T function particularly strongly limits the value of the entire approach. We therefore strongly encourage research that aims to develop approaches for obtaining more precise estimates of annual precipitation at ELAs. Additional work is needed before ELAs of small ice masses in mid-elevation mountainous regions in Central Europe can—if at all—be used for realistic and precise estimates of annual precipitation.

Supplementary Material. The supplementary material for this article can be found at https://doi.org/10.1017/qua.2023.53

Acknowledgments. This work was undertaken while Felix Martin Hofmann was in receipt of a PhD studentship of Studienstiftung des Deutschen Volkes. This study was financially supported by the German Research Foundation through the 'Geometry, chronology and dynamics of the last Pleistocene glaciation of the Black Forest' and 'Chronology of the glaciation of the Southern Black Forest after the Late Pleistocene glaciation maximum' projects granted to Frank Preusser (project numbers: 426333515 and 516126018, respectively). The French AMS national facility ASTER at CEREGE is supported by the INSU/CNRS, the ANR through the 'Projets thématiques d'excellence' programme for the 'Equipements d'excellence' ASTER-CEREGE action and IRD. We gratefully appreciate the help of Florian Rauscher and Oliver Kox during fieldwork. Alicia Sullivan is acknowledged for her help during sample preparation. The authors thank Irene Schimmelpfennig for her advice during sample preparation. Thanks are due to the State Geological Survey of Baden–Württemberg for providing LiDAR data of the study area. The nature protection department of Regierungspräsidium Freiburg and the forestry department of the Breisgau–Hochschwarzwald district, particularly Clemens Glunk and Jens-Uwe Strauch, are thanked for permission for sampling. The forestry department of the Breisgau–Hochschwarzwald district kindly provided a forest access permit. We express our gratitude to William McCreary III for performing a language check. We also thank the two reviewers and Yeong Bae Seong, the associate editor, for their very thoughtful and constructive comments, which resulted in considerable improvements to the manuscript.

REFERENCES

Arnold, M., Merchel, S., Bourlès, D.L., Braucher, R., Benedetti, L., Finkel, R.C., Aumaître, G., Gottdang, A., Klein, M., 2010. The French accelerator mass spectrometry facility ASTER: improved performance and developments. *Nuclear Instruments and Methods in Physics Research Section B: Beam Interactions with Materials and Atoms* **268**, 1954–1959.

Bakke, J., Nesje, A., 2011. Equilibrium-Line Altitude (ELA). In: Singh, V.P., Singh, P., Haritashya, U.K. (Eds.), *Encyclopedia of Snow, Ice and Glaciers*. Springer Netherlands, Dordrecht, pp. 268–277.

Balco, G., 2011. Contributions and unrealized potential contributions of cosmogenic-nuclide exposure dating to glacier chronology, 1990–2010. *Quaternary Science Reviews* **30**, 3–27.

Balco, G., Stone, J.O., Lifton, N.A., Dunai, T.J., 2008. A complete and easily accessible means of calculating surface exposure ages or erosion rates from ^{10}Be and ^{26}Al measurements. *Quaternary Geochronology* **3**, 174–195.

Ballantyne, C.K., 2007. The Loch Lomond Readvance on north Arran, Scotland: glacier reconstruction and palaeoclimatic implications. *Journal of Quaternary Science* **22**, 343–359.

Benn, D.I., Ballantyne, C.K., 2005. Palaeoclimatic reconstruction from Loch Lomond Readvance glaciers in the West Drumochter Hills, Scotland. *Journal of Quaternary Science* **20**, 577–592.

Benn, D.I., Hulton, N.R., 2010. An ExcelTM spreadsheet program for reconstructing the surface profile of former mountain glaciers and ice caps. *Computers & Geosciences* **36**, 605–610.

Bolland, A., Rey, F., Gobet, E., Tinner, W., Heiri, O., 2020. Summer temperature development 18,000–14,000 cal. BP recorded by a new chironomid record from Burgäschisee, Swiss Plateau. *Quaternary Science Reviews* **243**, 106484. https://doi.org/10.1016/j.quascirev.2020.106484 .

Boston, C.M., Lukas, S., Carr, S.J., 2015. A Younger Dryas plateau icefield in the Monadhliath, Scotland, and implications for regional palaeoclimate. *Quaternary Science Reviews* **108**, 139–162.

Boulton, G.S., Morris, E.M., Armstrong, A.A., Thomas, A., 1979. Direct measurement of stress at the base of a glacier. *Journal of Glaciology* **22**, 3–24.

Braithwaite, R.J., 2008. Temperature and precipitation climate at the equilibrium-line altitude of glaciers expressed by the degree-day factor for melting snow. *Journal of Glaciology* **54**, 437–444.

Braucher, R., Guillou, V., Bourlès, D.L., Arnold, M., Aumaître, G., Keddadouche, K., Nottoli, E., 2015. Preparation of ASTER in-house ^{10}Be/^{9}Be standard solutions. *Nuclear Instruments and Methods in Physics Research Section B: Beam Interactions with Materials and Atoms* **361**, 335–340.

Brown, E.T., Edmond, J.M., Raisbeck, G.M., Yiou, F., Kurz, M.D., Brook, E.J., 1991. Examination of surface exposure ages of Antarctic moraines using in situ produced ^{10}Be and ^{26}Al. *Geochimica et Cosmochimica Acta* **55**, 2269–2283.

Chandler, B.M., Boston, C.M., Lukas, S., 2019. A spatially-restricted Younger Dryas plateau icefield in the Gaick, Scotland: reconstruction and palaeoclimatic implications. *Quaternary Science Reviews* **211**, 107–135.

Chandler, B.M.P., Lukas, S., 2017. Reconstruction of Loch Lomond Stadial (Younger Dryas) glaciers on Ben More Coigach, north-west Scotland, and implications for reconstructing palaeoclimate using small ice masses. *Journal of Quaternary Science* **32**, 475–492.

Chmeleff, J., Blanckenburg, F. von, Kossert, K., Jakob, D., 2010. Determination of the ^{10}Be half-life by multicollector ICP-MS and liquid scintillation counting. *Nuclear Instruments and Methods in Physics Research Section B: Beam Interactions with Materials and Atoms* **268**, 192–199.

Clark, C.D., Ely, J.C., Hindmarsh, R.C.A., Bradley, S., Ignéczi, A., Fabel, D., Ó Cofaigh, C., et al., 2022. Growth and retreat of the last British–Irish Ice Sheet, 31 000 to 15 000 years ago: the BRITICE–CHRONO reconstruction. *Boreas* **51**, 699–758.

Claude, A., Ivy-Ochs, S., Kober, F., Antognini, M., Salcher, B., Kubik, P.W., 2014. The Chironico landslide (Valle Leventina, southern Swiss Alps): age and evolution. *Swiss Journal of Geosciences* **107**, 273–291.

Cohen, D., 2005. Debris-bed friction of hard-bedded glaciers. *Journal of Geophysical Research: Solid Earth* **110**, F02007. https://doi.org/10.1029/2004JF000228 .

Coleman, C.G., Carr, S.J., Parker, A.G., 2009. Modelling topoclimatic controls on palaeoglaciers: implications for inferring palaeoclimate from geomorphic evidence. *Quaternary Science Reviews* **28**, 249–259.

Dahl, S.O., Nesje, A., Øvstedal, J., 1997. Cirque glaciers as morphological evidence for a thin Younger Dryas ice sheet in east-central southern Norway. *Boreas* **26**, 161–180.

Denton, G.H., Alley, R.B., Comer, G.C., Broecker, W.S., 2005. The role of seasonality in abrupt climate change. *Quaternary Science Reviews* **24**, 1159–1182.

Denton, G.H., Anderson, R.F., Toggweiler, J.R., Edwards, R.L., Schaefer, J.M., Putnam, A.E., 2010. The last glacial termination. *Science* **328**, 1652–1656.

Earth Resources Observation and Science (EROS) Center, 2018. USGS EROS Archive – Digital Elevation – Shuttle Radar Topography Mission (SRTM) 1 Arc-Second Global. https://doi.org/10.5066/F7PR7TFT .

Eggermont, H., Heiri, O., 2012. The chironomid-temperature relationship: expression in nature and palaeoenvironmental implications. *Biological Reviews of the Cambridge Philosophical Society* **87**, 430–456.

Engel, Z., Braucher, R., Traczyk, A., Léanni, L., ASTER Team, 2014. ^{10}Be exposure age chronology of the last glaciation in the Krkonoše Mountains, Central Europe. *Geomorphology* **206**, 107–121.

Engel, Z., Traczyk, A., Braucher, R., Woronko, B., Křížek, M., 2011. Use of ^{10}Be exposure ages and Schmidt hammer data for correlation of moraines in the Krkonoše Mountains, Poland/Czech Republic. *Zeitschrift für Geomorphologie* **55**, 175–196.

Erb, L., 1948. Die Geologie des Feldbergs. In: Müller, K. (Ed.), *Der Feldberg im Schwarzwald. Naturwissenschaftliche, landwirtschaftliche, forstwirtschaftliche, geschichtliche und siedlungsgeschichtliche Studien*. L. Bielefelds Verlag KG, Freiburg i. Br., pp. 22–96.

Fezer, F., Günther, W., Reichelt, G., 1961. Plateauverfirnung und Talgletscher im Nordschwarzwald. *Abhandlungen der Braunschweigischen Wissenschaftlichen Gesellschaft* **13**, 66–72.

Florineth, D., Schlüchter, C., 2000. Alpine evidence for atmospheric circulation patterns in Europe during the Last Glacial Maximum. *Quaternary Research* **54**, 295–308.

Gaar, D., Graf, H.R., Preusser, F., 2019. New chronological constraints on the timing of Late Pleistocene glacier advances in northern Switzerland. *E&G Quaternary Science Journal* **68**, 53–73.

Geyer, O.F., Gwinner, M.P., 2011. *Geologie von Baden-Württemberg*, 5th ed. Schweizerbart, Stuttgart.

Giermann, G., 1964. Die würmeiszeitliche Vergletscherung des Schauinsland–Trubelsmattkopf–Knöpflesbrunnen-Massivs (südlicher Schwarzwald). *Berichte der Naturforschenden Gesellschaft zu Freiburg im Breisgau* **54**, 197–207.

Golledge, N., Hubbard, A., Bradwell, T., 2010. Influence of seasonality on glacier mass balance, and implications for palaeoclimate reconstructions. *Climate Dynamics* **35**, 757–770.

Golledge, N.R., Hubbard, A., Sugden, D.E., 2008. High-resolution numerical simulation of Younger Dryas glaciation in Scotland. *Quaternary Science Reviews* **27**, 888–904.

Gosse, J.C., Phillips, F.M., 2001. Terrestrial in situ cosmogenic nuclides: theory and application. *Quaternary Science Reviews* **20**, 1475–1560.

Graf, A., Akçar, N., Ivy-Ochs, S., Strasky, S., Kubik, P.W., Christl, M., Burkhard, M., Wieler, R., Schlüchter, C., 2015. Multiple advances of Alpine glaciers into the Jura Mountains in the Northwestern Switzerland. *Swiss Journal of Geosciences* **108**, 225–238.

Gribenski, N., Valla, P.G., Preusser, F., Roattino, T., Crouzet, C., Buoncristiani, J.-F., 2021. Out-of-phase Late Pleistocene glacial maxima in the Western Alps reflect past changes in North Atlantic atmospheric circulation. *Geology* **49**, 1096–1101.

Guiot, J., Pons, A., Beaulieu, J. L. de, Reille, M., 1989. A 140,000-year continental climate reconstruction from two European pollen records. *Nature* **338**, 309–313.

Hann, H.P., Schreiner, A., Zedler, H., 2011. *Geologische Karte von Baden-Württemberg 1:25 000. Blatt 8113 Todtnau*. 1:25,000. Landesamt für Geologie, Rohstoffe und Bergbau, Freiburg im Breisgau.

Heiri, O., Brooks, S.J., Renssen, H., Bedford, A., Hazekamp, M., Ilyashuk, B., Jeffers, E.S., *et al.*, 2014b. Validation of climate model-inferred regional temperature change for late-glacial Europe. *Nature Communications* **5**, 4914. https://doi.org/10.1038/ncomms5914 .

Heiri, O., Ilyashuk, B., Millet, L., Samartin, S., Lotter, A.F., 2015. Stacking of discontinuous regional palaeoclimate records: chironomid-based summer temperatures from the Alpine region. *The Holocene* **25**, 137–149.

Heiri, O., Koinig, K.A., Spötl, C., Barrett, S., Brauer, A., Drescher-Schneider, R., Gaar, D., *et al.*, 2014a. Palaeoclimate records 60–8 ka in the Austrian and Swiss Alps and their forelands. *Quaternary Science Reviews* **106**, 186–205.

Heiri, O., Millet, L., 2005. Reconstruction of Late Glacial summer temperatures from chironomid assemblages in Lac Lautrey (Jura, France). *Journal of Quaternary Science* **20**, 33–44.

Hemmerle, H., May, J.-H., Preusser, F., 2016. Übersicht über die pleistozänen Vergletscherungen des Schwarzwaldes. *Berichte der Naturforschenden Gesellschaft zu Freiburg im Breisgau* **106**, 31–67.

Heyman, B.M., Heyman, J., Fickert, T., Harbor, J.M., 2013. Paleo-climate of the central European uplands during the last glacial maximum based on glacier mass-balance modeling. *Quaternary Research* **79**, 49–54.

Hofmann, F.M., 2022. Technical note: evaluating a geographical information system (GIS)- based approach for determining topographic shielding factors in cosmic-ray exposure dating. *Geochronology* **4**, 691–712.

Hofmann, F.M., Preusser, F., Schimmelpfennig, I., Léanni, L., ASTER Team, 2022. Late Pleistocene glaciation history of the southern Black Forest, Germany: ^{10}Be cosmic-ray exposure dating and equilibrium-line altitude reconstructions in Sankt Wilhelmer Tal. *Journal of Quaternary Science* **37**, 688–706.

Hofmann, F.M., Rauscher, F., McCreary, W., Bischoff, J.P., Preusser, F., 2020. Revisiting Late Pleistocene glacier dynamics north-west of the Feldberg, southern Black Forest, Germany. *E&G Quaternary Science Journal* **69**, 61–87.

Hughes, P.D., Braithwaite, R.J., 2008. Application of a degree-day model to reconstruct Pleistocene glacial climates. *Quaternary Research* **69**, 110–116.

Hughes, P.D., Gibbard, P.L., 2015. A stratigraphical basis for the Last Glacial Maximum (LGM). *Quaternary International* **383**, 174–185.

Hüttner, R., 1967. Das Quartär. In: Geologisches Landesamt Baden–Württemberg (Ed.), Geologische Karte von Baden-Württemberg 1:25 000, Erläuterungen zu Blatt 8013 Freiburg-Südost. Landesvermessungsamt Baden–Württemberg, Stuttgart, pp. 69–105.

Isarin, R.F., Renssen, H., 1999. Reconstructing and modelling Late Weichselian climates: the Younger Dryas in Europe as a case study. *Earth-Science Reviews* **48**, 1–38.

Isarin, R.F., Renssen, H., Vandenberghe, J., 1998. The impact of the North Atlantic Ocean on the Younger Dryas climate in northwestern and central Europe. *Journal of Quaternary Science* **13**, 447–453.

Ivanov, M.N., 2012. *Polar Urals Glaciers and Periglacial Geomorphology. TICOP Excursion Guidebook*. Pechatnik, Tyumen, Russia.

Ivy-Ochs, S., Kerschner, H., Reuther, A., Preusser, F., Heine, K., Maisch, M., Kubik, P.W., Schlüchter, C., 2008. Chronology of the last glacial cycle in the European Alps. *Journal of Quaternary Science* **23**, 559–573.

Ivy-Ochs, S., Monegato, G., Reitner, J.M., 2023. The Alps: glacial landforms from the Younger Dryas Stadial. In: Palacios, D., Hughes, P.D., García Ruiz, J.M., Andrés, N. (Eds.), *European Glacial Landscapes. The Last Deglaciation*. Elsevier, Amsterdam, Oxford, Cambridge, pp. 525–539.

Jarvis, A., Reuter, H.I., Nelson, A., Guevara, E., 2008. Hole-filled seamless SRTM data V4 (SRTM 90m DEM Digital Elevation Database). http://srtm.csi.cgiar.org.

Korschinek, G., Bergmaier, A., Faestermann, T., Gerstmann, U.C., Knie, K., Rugel, G., Wallner, A., *et al.*, 2010. A new value for the half-life of ^{10}Be by heavy-ion elastic recoil detection and liquid scintillation counting. *Nuclear Instruments and Methods in Physics Research Section B: Beam Interactions with Materials and Atoms* **268**, 187–191.

Kuhlemann, J., Rohling, E.J., Krumrei, I., Kubik, P., Ivy-Ochs, S., Kucera, M., 2008. Regional synthesis of Mediterranean atmospheric circulation during the Last Glacial Maximum. *Science* **321**, 1338–1340.

Kuttler, W., 2013. *Klimatologie*, 2nd ed. Schöningh, Paderborn, Germany.

Lal, D., 1991. Cosmic ray labeling of erosion surfaces: in situ nuclide production rates and erosion models. *Earth and Planetary Science Letters* **104**, 424–439.

Lang, G., 2005. *Seen und Moore des Schwarzwaldes als Zeugen spätglazialen und holozänen Vegetationswandels. Stratigraphische, pollenanalytische und großrestanalytische Untersuchungen*. Staatliches Museum für Naturkunde Karlsruhe, Karlsruhe.

Larocque-Tobler, I., Heiri, O., Wehrli, M., 2010. Late Glacial and Holocene temperature changes at Egelsee, Switzerland, reconstructed using subfossil chironomids. *Journal of Paleolimnology* **43**, 649–666.

Liehl, E., 1975. Geländeformen des Feldberggebiets. In: Hofmann, W., Louis, H. (Eds.), *Landformen im Kartenbild. Topographisch-Geomorphologische*

https://doi.org/10.1017/qua.2023.53 Published online by Cambridge University Press

Kartenproben 1: 25 000. Gruppe II: Mittelgebirge. Gefalteter Unterbau, stellenweise überlagert. Kartenprobe 6: Kristalliner Schwarzwald mit Karen und Moränen, Feldberg. Westermann, Braunschweig, Germany, pp. 8–16.

Liehl, E., 1982. Landschaftsgeschichte des Feldberggebietes. Altlandschaft–Eiszeit–Verwitterung und Abtragung heute. In: Landesanstalt für Umweltschutz Baden–Württemberg – Institut für Ökologie und Naturschutz (Ed.), Der Feldberg im Schwarzwald: Subalpine Insel im Mittelgebirge. Institut für Ökologie und Naturschutz, Karlsruhe, Germany 12, 13–147.

Lisiecki, L.E., Raymo, M.E., 2005. A Pliocene–Pleistocene stack of 57 globally distributed benthic $\delta^{18}O$ records. *Paleoceanography* **20**, PA1003. https://doi.org/10.1029/2004PA001071 .

Li, Y.-K., 2013. Determining topographic shielding from digital elevation models for cosmogenic nuclide analysis: a GIS approach and field validation. *Journal of Mountain Science* **10**, 355–362.

Li, Y.-K., 2018. Determining topographic shielding from digital elevation models for cosmogenic nuclide analysis: a GIS model for discrete sample sites. *Journal of Mountain Science* **15**, 939–947.

Mackintosh, A.N., Anderson, B.M., Pierrehumbert, R.T., 2017. Reconstructing climate from glaciers. *Annual Review of Earth and Planetary Sciences* **45**, 649–680.

Magny, M., Aalbersberg, G., Bégeot, C., Benoit-Ruffaldi, P., Bossuet, G., Disnar, J.-R., Heiri, O., *et al.*, 2006. Environmental and climatic changes in the Jura mountains (eastern France) during the Lateglacial–Holocene transition: a multi-proxy record from Lake Lautrey. *Quaternary Science Reviews* **25**, 414– 445.

Magny, M., Guiot, J., Schoellammer, P., 2001. Quantitative reconstruction of Younger Dryas to Mid-Holocene paleoclimates at Le Locle, Swiss Jura, using pollen and lake-level data. *Quaternary Research* **56**, 170–180.

Mangerud, J., 2021. The discovery of the Younger Dryas, and comments on the current meaning and usage of the term. *Boreas* **50**, 1–5.

Mangerud, J., Gosse, J., Matiouchkov, A., Dolvik, T., 2008. Glaciers in the Polar Urals, Russia, were not much larger during the Last Global Glacial Maximum than today. *Quaternary Science Reviews* **27**, 1047–1057.

Martin, L.C.P., Blard, P.H., Balco, G., Lavé, J., Delunel, R., Lifton, N., Laurent, V., 2017. The CREp program and the ICE-D production rate calibration database: a fully parameterizable and updated online tool to compute cosmic-ray exposure ages. *Quaternary Geochronology* **38**, 25–49.

Masarik, J., Wieler, R., 2003. Production rates of cosmogenic nuclides in boulders. *Earth and Planetary Science Letters* **216**, 201–208.

Matzarakis, A., 2012. Klima. In: Regierungspräsidium Freiburg (Ed.), Der Feldberg: subalpine Insel im Schwarzwald. Jan Thorbecke Verlag der Schwabenverlag AG, Ostfildern, Germany, pp. 95–106.

Mentlík, P., Engel, Z., Braucher, R., Léanni, L., ASTER Team, 2013. Chronology of the Late Weichselian glaciation in the Bohemian Forest in Central Europe. *Quaternary Science Reviews* **65**, 120–128.

Merchel, S., Herpers, U., 1999. An update on radiochemical separation techniques for the determination of long-lived radionuclides via accelerator mass spectrometry. *Radiochimica Acta* **84**, 215–220.

Mercier, J.-L., Bourlès, D.L., Kalvoda, J., Braucher, R., Paschen, A., 1999. Deglaciation of the Vosges dated using ^{10}Be. *Acta Universitatis Carolinae Geographica* **2**, 139–155.

Mercier, J.-L., Kalvoda, J., Bourlès, D.L., Braucher, R., Engel, Z., 2000. Preliminary results of ^{10}Be dating of glacial landscape in the Giant Mountains. *Acta Universitatis Carolinae Geographica, Supplementum* **35**, 157–170.

Metz, B., 1985a. *Geomorphologische Karte 1:25 000 der Bundesrepublik Deutschland. GMK 25 Blatt 21. 8114 Feldberg*. GMK-Schwerpunktprogramm der Deutschen Forschungsgemeinschaft (DFG), Berlin.

Metz, B., 1985b. *Erläuterungen zur Geomorphologischen Karte 1:25 000 der Bundesrepublik Deutschland, GMK 25 Blatt 21, 8114 Feldberg*. Berlin.

Metz, B., Saurer, H., 2012. Geomorphologie und Landschaftsentwicklung. In: Regierungspräsidium Freiburg (Ed.), Der Feldberg: Subalpine Insel im Schwarzwald. Jan Thorbecke Verlag der Schwabenverlag AG, Ostfildern, Germany, pp. 14–62.

Mills, S.C., Grab, S.W., Carr, S.J., 2009. Recognition and palaeoclimatic implications of late Quaternary niche glaciation in eastern Lesotho. *Journal of Quaternary Science* **24**, 647–663.

Mills, S.C., Grab, S.W., Rea, B.R., Carr, S.J., Farrow, A., 2012. Shifting westerlies and precipitation patterns during the Late Pleistocene in southern Africa determined using glacier reconstruction and mass balance modelling. *Quaternary Science Reviews* **55**, 145–159.

Mitchell, W.A., 1996. Significance of snowblow in the generation of Loch Lomond Stadial (Younger Dryas) glaciers in the western Pennines, northern England. *Journal of Quaternary Science* **11**, 233–248.

Monegato, G., Scardia, G., Hajdas, I., Rizzini, F., Piccin, A., 2017. The Alpine LGM in the boreal ice-sheets game. *Scientific Reports* **7**, 2078. https://doi.org/10.1038/s41598-017-02148-7 .

Muscheler, R., Beer, J., Kubik, P.W., Synal, H.A., 2005. Geomagnetic field intensity during the last 60,000 years based on ^{10}Be and ^{36}Cl from the Summit ice cores and ^{14}C. *Quaternary Science Reviews* **24**, 1849–1860.

Naughton, F., Sánchez-Goñi, M.F., Landais, A., Rodrigues, T., Riveiros, N.V., Toucanne, S., 2023. The Younger Dryas Stadial. In: Palacios, D., Hughes, P.D., García Ruiz, J.M., Andrés, N. (Eds.), *European Glacial Landscapes. The Last Deglaciation*. Elsevier, Amsterdam, Oxford, Cambridge, pp. 51–57.

Nishiizumi, K., Imamura, I., Caffee, M.W., Southon, J.R., Finkel, R.C., McAninch, J., 2007. Absolute calibration of ^{10}Be AMS standards. *Nuclear Instruments and Methods in Physics Research Section B: Beam Interactions with Materials and Atoms* **258**, 403–413.

Nishiizumi, K., Winterer, E.L., Kohl, C.P., Klein, J., Middleton, R., Lal, D., Arnold, J.R., 1989. Cosmic ray production rates of ^{10}Be and ^{26}Al in quartz from glacially polished rocks. *Journal of Geophysical Research: Solid Earth* **94**, 17907–17915.

Ohmura, A., Boettcher, M., 2018. Climate on the equilibrium-line altitudes of glaciers: theoretical background behind Ahlmann's P/T diagram. *Journal of Glaciology* **64**, 489–505.

Ohmura, A., Kasser, P., Funk, M., 1992. Climate at the equilibrium-line of glaciers. *Journal of Glaciology* **38**, 397–411.

Oien, R.P., Rea, B.R., Spagnolo, M., Barr, I.D., Bingham, R.G., 2022. Testing the area–altitude balance ratio (AABR) and accumulation–area ratio (AAR) methods of calculating glacier equilibrium-line altitudes. *Journal of Glaciology* **68**, 357–368.

Osmaston, H., 2005. Estimates of glacier equilibrium-line altitudes by the area × altitude, the area × altitude balance ratio and the area × altitude balance index methods and their validation. *Quaternary International* 138–139, 22–31.

Palacios, D., Hughes, P.D., García Ruiz, J.M., Andrés, N. (Eds.), 2023. *European Glacial Landscapes. The Last Deglaciation*. Elsevier, Amsterdam, Oxford, Cambridge.

Parlow, E., Rosner, H.-J., 1997. Das Klima des Oberrheingrabens. In: Mäckel, R., Metz, B. (Eds.), *Schwarzwald und Oberrheintiefland. Eine Einführung in das Exkursionsgebiet. Freiburg im Breisgau*. Freiburger Geographische Hefte 36, 111–124.

Paterson, W.S.B., 1970. The sliding velocity of Athabasca Glacier, Canada. *Journal of Glaciology* **9**, 55–63.

Pearce, D.M., Ely, J.C., Barr, I.D., Boston, C.M., 2017. Glacier reconstruction. In: Clarke, L.E., Nield, J.M. (Eds.), *Geomorphological Techniques*. British Society for Geomorphology, London.

Pellitero, R., Rea, B.R., Spagnolo, M., Bakke, J., Hughes, P., Ivy-Ochs, S., Lukas, S., Ribolini, A., 2015. A GIS tool for automatic calculation of glacier equilibrium-line altitudes. *Computers & Geosciences* **82**, 55–62.

Pellitero, R., Rea, B.R., Spagnolo, M., Bakke, J., Ivy-Ochs, S., Frew, C.R., Hughes, P., Ribolini, A., Lukas, S., Renssen, H., 2016. GlaRe, a GIS tool to reconstruct the 3D surface of palaeoglaciers. *Computers & Geosciences* **94**, 77–85.

Peyron, O., Bégeot, C., Brewer, S., Heiri, O., Magny, M., Millet, L., Ruffaldi, P., van Campo, E., Yu, G., 2005. Late-Glacial climatic changes in eastern France (Lake Lautrey) from pollen, lake-levels, and chironomids. *Quaternary Research* **64**, 197–211.

Plummer, M.A., Phillips, F.M., 2003. A 2-D numerical model of snow/ice energy balance and ice flow for paleoclimatic interpretation of glacial geomorphic features. *Quaternary Science Reviews* **22**, 1389–1406.

Ponel, P., 1995. Rissian, Eemian and Würmian Coleoptera assemblages from La Grande Pile (Vosges, France). *Palaeogeography, Palaeoclimatology, Palaeoecology* **114**, 1–41.

Rahm, G., 1987. Die Vergletscherung des Belchengebietes (Südschwarzwald) zur Würmeiszeit. *E&G Quaternary Science Journal* **37**, 31–40.

https://doi.org/10.1017/qua.2023.53 Published online by Cambridge University Press

Rasmussen, S.O., Bigler, M., Blockley, S.P., Blunier, T., Buchardt, S.L., Clausen, H.B., Cvijanovic, I., *et al.* 2014. A stratigraphic framework for abrupt climatic changes during the Last Glacial period based on three synchronized Greenland ice-core records: refining and extending the INTIMATE event stratigraphy. *Quaternary Science Reviews* **106**, 14–28.

Rea, B.R., 2009. Defining modern day area-altitude balance ratios (AABRs) and their use in glacier-climate reconstructions. *Quaternary Science Reviews* **28**, 237–248.

Rea, B.R., Pellitero, R., Spagnolo, M., Hughes, P., Ivy-Ochs, S., Renssen, H., Ribolini, A., Bakke, J., Lukas, S., Braithwaite, R.J., 2020. Atmospheric circulation over Europe during the Younger Dryas. *Science Advances* **6**, eaba4844. https://doi.org/10.1126/sciadv.aba4844 .

Reichelt, G., 1996. Zum eiszeitlichen Geschehen im Mittelschwarzwald. Interpretation einer geomorphologischen Karte. *Schriften des Vereins für Geschichte und Naturgeschichte der Baar* **39**, 182–189.

Renssen, H., Isarin, R., 2001. The two major warming phases of the last deglaciation at ∼14.7 and ∼11.5 ka cal BP in Europe: climate reconstructions and AGCM experiments. *Global and Planetary Change* **30**, 117–153.

Renssen, H., Kasse, C., Vandenberghe, J., Lorenz, S.J., 2007. Weichselian late pleniglacial surface winds over northwest and central Europe: a model–data comparison. *Journal of Quaternary Science* **22**, 281–293.

Reuther, A.U., 2007. *Surface exposure dating of glacial deposits from the last glacial cycle. Evidence from the Eastern Alps, the Bavarian Forest, the Southern Carpathians and the Altai Mountains*. Relief Boden Paläoklima 21, 213 pp.

Sawatzki, G., 1992. *Geologische Karte 1:25 000 von Baden-Württemberg. Erläuterungen zu Blatt 8214 St. Blasien*. Landesvermessungsamt Baden-Württemberg, Stuttgart.

Schenk, F., Väliranta, M., Muschitiello, F., Tarasov, L., Heikkilä, M., Björck, S., Brandefelt, J., Johansson, A.V., Näslund, J.-O., Wohlfarth, B., 2018. Warm summers during the Younger Dryas cold reversal. *Nature Communications* **9**, 1634. https://doi.org/10.1038/s41467-018-04071-5 .

Schreiner, A., 1977. *Geologische Karte von Baden-Württemberg 1:50 000. Freiburg i. Br. und Umgebung*, 1st ed. Geologisches Landesamt Baden-Württemberg, Freiburg i. Br.

Schreiner, A., 1996. *Geologische Karte von Baden-Württemberg 1:50 000. Freiburg i. Br. und Umgebung*, 3rd ed. Geologisches Landesamt Baden-Württemberg, Freiburg i. Br.

Sissons, J.B., 1974. A Late-Glacial ice cap in the Central Grampians, Scotland. *Transactions of the Institute of British Geographers* **62**, 95–114.

Sissons, J.B., 1980. The Loch Lomond Advance in the Lake District, northern England. *Transactions of the Royal Society of Edinburgh: Earth Sciences* **71**, 13–27.

Steinmann, G., 1902. Die Bildungen der letzten Eiszeit im Bereiche des alten Wutachgebiets. *Berichte des Oberrheinischen Geologischen Vereins* **35**, 1–8.

Steinmann, G., 1910. *Die Eiszeit und der vorgeschichtliche Mensch*. B. G. Teubner, Leipzig.

Stone, J.O., 2000. Air pressure and cosmogenic isotope production. *Journal of Geophysical Research: Solid Earth* **105**, 23753–23759.

Svendsen, J.I., Mangerud, J., Nazarov, D., Regnéll, C., 2023. Glacial landscapes of the Ural Mountains. In: Palacios, D., Hughes, P.D., García Ruiz, J.M., Andrés, N. (Eds.), *European Glacial Landscapes. Maximum Extent of Glaciations*. Elsevier, Amsterdam, Oxford, Cambridge, pp. 89–94.

Uppala, S.M., Kållberg, P.W., Simmons, A.J., Andrae, U., Da Bechtold, V.C., Fiorino, M., Gibson, J.K., *et al.*, 2005. The ERA-40 re-analysis. *Quarterly Journal of the Royal Meteorological Society* **131**, 2961–3012.

Voloshina, A.P., 1988. Some results of glacier mass balance research on the glaciers of the Polar Urals. *Polar Geography and Geology* **12**, 200–211.

Wimmenauer, W., Liehl, E., Schreiner, A., 1990. *Geologische Karte von Baden-Württemberg 1:25 000. Blatt 8114 Feldberg*, 2nd ed. Landesvermessungsamt Baden-Württemberg, Stuttgart.

Ziegler, P., 1992. European Cenozoic rift system. *Tectonophysics* **208**, 91–111.

Zienert, A., 1973. Die Würm-Vereisung und ihre Rückzugsstadien im Westteil des Hochschwarzwaldes. *Zeitschrift für Geomorphologie* **17**, 359–366.

Zienert, A., Fezer, F., 1967. Vogesen- und Schwarzwald-Kare. *E&G Quaternary Science Journal* **18**, 51–75.

Zweck, C., Zreda, M., Desilets, D., 2013. Snow shielding factors for cosmogenic nuclide dating inferred from Monte Carlo neutron transport simulations. *Earth and Planetary Science Letters* **379**, 64–71.

https://doi.org/10.1017/qua.2023.53 Published online by Cambridge University Press